AD-A040 618   TEXAS A AND M UNIV COLLEGE STATION MECHANICS AND MAT--ETC   F/G 11/4
ON MICROCRACK GROWTH AND ARREST IN SIMULATED FIRROUS COMPOSITES--ETC(U)
DEC 76   N CONRAD   N00014-75-C-0325

UNCLASSIFIED   MM-3168-76-10   NL
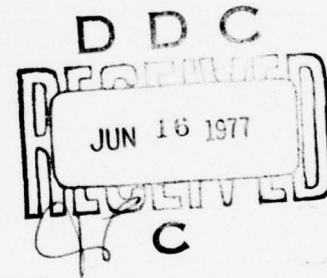
1 OF 2
ADA
040618

Mechanics and Materials Research Center
TEXAS A&M UNIVERSITY
College Station, Texas

ON MICROCRACK GROWTH AND ARREST IN SIMULATED FIBROUS COMPOSITES

NICHOLAS CONRAD

MM 3168-76-10

December 1976

Mechanics and Materials Research Center

Texas Engineering Experiment Station

TEXAS A&M UNIVERSITY

College Station, Texas 77843

ON MICROCRACK GROWTH AND ARREST

IN SIMULATED FIBROUS COMPOSITES

by

Nicholas Conrad

MM 3168-76-10

(See 1473)

December 1976

ABSTRACT*

     Opening, shearing and combined mode fracture tests were conducted
with long rectangular strips of plexiglas clamped on the long edges and
containing centered and off-centered cracks. The critical stress inten-
sity factors, crack initiation angles, and crack paths were evaluated.
Fractured surfaces were then examined as to crack behavior. The maximum
energy release rate criterion was extended to problems with a large
degree of shearing mode present. This criterion was then used to predict
successfully the initial and subsequent crack propagation behavior pre-
sented in the experimental work. Crack arrest was examined for this
rigid grip configuration. Using in part information obtained from these
studies, a flexible fiber model was investigated to determine the effect
of fiber bending on crack behavior. Certain aspects of crack growth and
arrest in these idealized fiber models were explored.

TABLE OF CONTENTS

LIST OF TABLES

LIST OF FIGURES

INTRODUCTION

In recent years, there has been an increased interest in the use of composite materials, though the idea of a composite or multi-phase material is centuries old [1]. There are two general groups of composite materials, particulate and fibrous, depending on the form of the added material [2]. This discussion will be limited to fibrous composites, consisting of stiff, approximately parallel fibers in a softer matrix material, as in Figure 1. The result is an efficient structural material. Current research is leading to the use of unusually strong, high modulus fibers of various materials with polymeric, ceramic, or metallic matrices, with resultant high strength-to-weight characteristics [3,4]. The most commonly used structural composite, however, consists of graphite or glass fibers in an epoxy matrix.

These constituent materials are usually considered to exhibit linear elastic behavior; however, the matrix and composite may exhibit a significant amount of time and temperature dependent mechanical behavior in many applications. To insure safe structural use of these materials, the elastic behavior must be examined, then extensions to viscoelasticity made. Much research on polymeric composites has been done in this manner [4,5].

Researchers have also found that polymeric composites are nonlinearly viscoelastic. Tsai et al. [4], Lou and Schapery [6], Ashton [7], and Schapery et al. [8] have shown these composites are not linear except at very small stress levels, which may be below structural design limits. Studies with fibrous composites indicate that
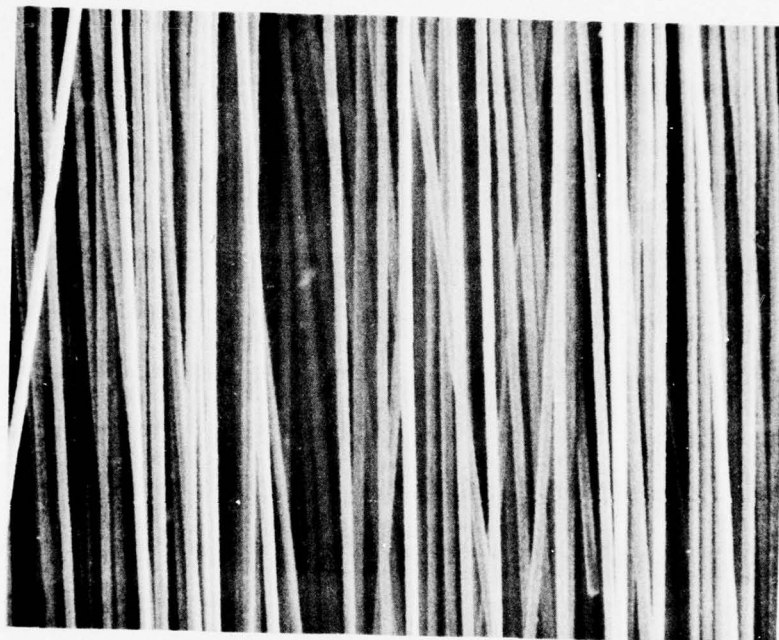
Figure 1.   Fibrous composite, HT-S/ERLA 2256 (300X).

a sizable portion of this nonlinearity is due to internal crack growth within the matrix or fiber/matrix interface [6,8,9]. This nonlinearity due to crack growth is significant, particularly during the first one or two cycles of loading and unloading of the structure, where a significant amount of irreversible damage occurs. However, except at high stresses or temperature, after these initial cycles the response does not change, probably indicating some sort of crack arrest [6,10,11].

The majority of the cracks originate as microscopic flaws in the matrix material resulting from the manufacturing of the composite structure [12-15]. Upon loading these defects cause stress concentrations, inducing crack initiation and growth. These cracks then propagate under load (even below catastrophic levels) in the matrix through various mechanisms [16-18].

The nature of crack propagation in the matrix is very complex. Geometrically, the microcrack in the matrix is at some angle to the surrounding fibers which are also at some other angle to the applied loading. The problem of a crack in a low modulus material surrounded by a much stiffer material (microcrack in the matrix of an advanced composite) has been investigated theoretically [18-21]. This research has shown that either the arbitrary crack propagates toward the stiffer material, causing the stress intensity factor to drop, forcing the crack to slow or arrest, or the crack may actually propagate toward the center of the matrix and then parallel to the fibers.

The direction of the fibers relative to an applied tensile load may have a significant affect on the tendency for microcrack arrest whether or not the crack is parallel to the fibers: indeed, as we will

show a crack which is initially aligned with the fibers could turn into the fibers with subsequent arrest if the shear stress along the fiber direction falls within a certain range.

Researchers have presented another possible mechanism of crack arrest, prevalent even with cracks parallel to the fibers. Fiber bending may cause cracks to then "skip" across the fiber and continue propagation in the same plane as the original crack [8,22,23] forming a crack arrest-growth mechanism.

The engineering theories of fracture mechanics can be used to investigate the nature of the crack arrest mechanisms on a micro-structural scale in composite materials. The work presented here starts with a review of the classical theory of fracture for a crack at an arbitrary orientation relative to the applied loads. Experimental data are then presented for a geometry similar to a cracked matrix surrounded by perfectly rigid fibers. Fracture mechanics, experimental data, and fractography data are compared. A cracked-composite model is then examined through a fracture mechanics approach to investigate some of the effects of fiber deformation in fibrous composite materials.

REVIEW OF SOME ASPECTS OF FRACTURE MECHANICS

General Development

The study of cracks, whether large or small, and their affect on structural or material behavior is generally entitled fracture mechanics. Fracture mechanics is often studied assuming linear elastic behavior, neglecting, for example, the nonlinear effects occurring in a small region about the crack tip. However, there are many investigations which treat plasticity and viscoelastic effects [e.g. 24, 25].

The formal study of fracture mechanics started with Griffith [26]. He used a linear, elastic stress solution provided by Inglis [27] for a flat plate under uniform tension with an elliptical hole, which was then degenerated into a crack. Without using the near tip stress field directly, Griffith devised an energy-rate analysis for the prediction of initiation of crack growth in brittle materials. Not until Sneddon were the stress-field expansions for the crack tips analyzed [28]. The general applicability of these field equations were recognized later by Irwin [29,30] and Williams [31], and expanded to a general form for the isotropic elastic body.

Using the methods of Westergaard [32], Irwin [33] derived three sets of equations describing three basic types of displacement fields as shown in Figure 2. The opening mode is associated with a local displacement in which the crack surfaces move directly apart, normal to the x-z plane. The anti-symmetric or sliding mode is characterized by displacements in which the crack surfaces slide over one another perpendicular to the leading edge of the crack. The third mode, skew symmetric or tearing, is described by the crack surfaces moving past one
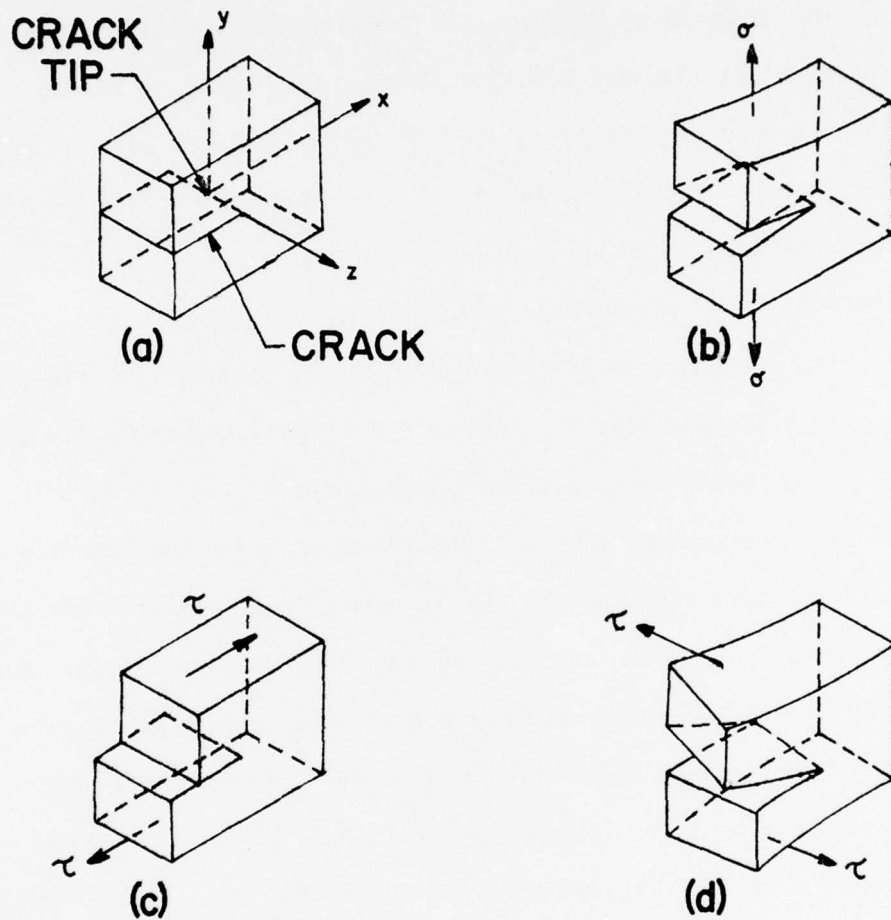
Figure 2. Three modes of crack surface displacements,
(a) crack in stress free body, (b) crack in the
opening mode, (c) crack in the anti-symmetric mode,
(d) crack in the skew-symmetric mode [13].

another parallel to the leading edge of the crack. Irwin's equations
for the local stresses and displacements (with r,θ the local polar
coordinates in the x-y plane) are:

Mode I

$$\sigma_{xx} = \frac{K_I}{(2\pi r)^{1/2}} \cos \frac{\theta}{2} (1 - \sin \frac{\theta}{2} \sin \frac{3\theta}{2}) + \ldots$$

$$\sigma_{yy} = \frac{K_I}{(2\pi r)^{1/2}} \cos \frac{\theta}{2} (1 + \sin \frac{\theta}{2} \sin \frac{3\theta}{2}) + \ldots$$

$$\sigma_{xy} = \frac{K_I}{(2\pi r)^{1/2}} \sin \frac{\theta}{2} \cos \frac{\theta}{2} \cos \frac{3\theta}{2} + \ldots$$

$$\sigma_{zz} = \nu(\sigma_{xx} + \sigma_{yy}) \quad , \quad \sigma_{xz} = \sigma_{yz} = 0 \tag{1}$$

$$u = \frac{K_I}{G} \left(\frac{r}{2\pi}\right)^{1/2} \cos \frac{\theta}{2} (1 - 2\nu + \sin^2 \frac{\theta}{2}) + \ldots$$

$$v = \frac{K_I}{G} \left(\frac{r}{2\pi}\right)^{1/2} \sin \frac{\theta}{2} (2 - 2\nu - \cos^2 \frac{\theta}{2}) + \ldots$$

$$w = 0$$

Mode II

$$\sigma_{xx} = \frac{-K_{II}}{(2\pi r)^{1/2}} \sin \frac{\theta}{2} (2 + \cos \frac{\theta}{2} \cos \frac{3\theta}{2}) + \ldots \ldots$$

$$\sigma_{yy} = \frac{K_{II}}{(2\pi r)^{1/2}} \sin \frac{\theta}{2} \cos \frac{\theta}{2} \cos \frac{3\theta}{2} + \ldots \ldots$$

$$\sigma_{xy} = \frac{K_{II}}{(2\pi r)^{1/2}} \cos \frac{\theta}{2} (1 - \sin \frac{\theta}{2} \sin \frac{3\theta}{2}) + \ldots \ldots$$

$$\sigma_{zz} = \nu(\sigma_{xx} + \sigma_{yy}) \quad , \quad \sigma_{xz} = \sigma_{yz} = 0 \tag{2}$$

$$u = \frac{K_{II}}{G} (\frac{r}{2\pi})^{1/2} \sin \frac{\theta}{2} (2 - 2\nu + \cos^2 \frac{\theta}{2}) + \ldots \ldots$$

$$v = \frac{K_{II}}{G} (\frac{r}{2\pi})^{1/2} \cos \frac{\theta}{2} (-1 + 2\nu + \sin^2 \frac{\theta}{2}) + \ldots \ldots$$

$$w = 0$$

Mode III

$$\sigma_{xy} = \frac{-K_{III}}{(2\pi r)^{1/2}} \sin \frac{\theta}{2} + \ldots \ldots$$

$$\sigma_{yz} = \frac{K_{III}}{(2\pi r)^{1/2}} \cos \frac{\theta}{2} + \ldots \ldots$$

$$\sigma_{xx} = \sigma_{yy} = \sigma_{zz} = \sigma_{xy} = 0 \tag{3}$$

$$w = \frac{K_{III}}{G} (\frac{2r}{\pi})^{1/2} \sin \frac{\theta}{2} + \ldots \ldots$$

$$u = v = 0$$

Each of these equations contains only the first term of an expansion about the crack tip and is exact as r approaches zero. Since it has been generally believed and shown by others [34] that the region about the crack tip is in a state of plane strain, the first two sets of equations are written for this case.

The K's in the above equations are parameters called stress intensity factors. As these factors are not dependent on the local coordinates (r, θ), they control the intensity of the stress field, not the shape of it. These factors depend on the magnitude of the applied forces and the geometry of the body containing the crack, or cracks, including crack size [35,36]. Their values can be calculated from analyses that are either three-dimensional, plane stress or plane strain, depending on the problem being considered. This leads to confusion since the crack tip region is considered to be in plane strain [34, 37]. This paradox is due to the attempt to investigate a locally three-dimensional problem using two-dimensional concepts. Since these parameters are functions of the applied loads, their values at failure are considered as "critical" stress intensity factors. These values then can be determined by experiments. Since the inception of the stress-intensity factor approach, many geometries have been analyzed [e.g., see 37,38]. Due to limitations of analytical techniques, only relatively simple geometries have been analyzed.

Numerical Analysis in Fracture Mechanics

Cracked structures rarely have simple crack geometries. This has lead to an increased amount of research in the area of numerical techniques needed to analyze cracked bodies. Boundary collocation

schemes and finite element methods have been the major approaches.

The boundary collocation technique will be discussed first. This technique starts with a stress function which is used to describe the stresses throughout a cracked body and satifies the boundary conditions at discrete points. This procedure offers some advantages over other methods such as little data preparation, great accuracy, and a smaller number of equations to be solved [39,40]. The collocation technique does not have the flexibility of other methods in that of allowing curved cracks, complex external boundaries and complicated loading conditions.

Due to its flexibility, the finite element method has been used extensively in fracture analysis. The finite element method itself is well documented and will not be discussed here [41]. However, a brief review of the various approaches to fracture mechanics with the use of finite elements will be presented.

One approach is called the displacement method. Displacements are obtained from a model with a coarse outer grid and a very fine grid near the crack tip. By using the calculated nodal displacements along the crack face and the displacement equations about a crack tip, described previously, a stress intensity factor can be estimated from each nodal point. Since the displacements are not exact, a curve of estimated K's versus the location of the nodal point with respect to the crack tip is obtained, rather than a single value for K. Chan et al. [42] have found that the curve appeared to be linear some distance from the crack tip, the distance decreasing with increased grid refinement. A tangential extrapolation on the curve

to the crack tip was used to estimate K. The answers obtained in this manner can be reasonably accurate (<5% error) but only with very refined meshes (elements on the order of element area/crack length squared, (3.2×10^6) [42]. Obviously, this method is not very precise in execution and very costly by requiring such fine meshes.

Others [43,44] have added higher order terms to the local crack tip displacement equations with some success. Using the logic that as the calculated displacements increase in accuracy and the local displacement equations decrease in accuracy as one moves from the crack tip, a suitable compromise might be achieved. Plotting as before, a maximum K can be found and can also be fairly accurate (<5% error). Mesh refinement is still a problem as is the preciseness of execution.

A novel approach, also using displacements, has recently been proposed [45]. This method is based on using the calculated nodal displacements to plot the deformed shape of the crack and compare it to the ellipse predicted by an elastic fracture mechanics analysis for an elliptical crack. This method is also limited in requiring some mesh refinement and is only applicable to opening mode cracks.

An approach similar to the displacement method is based on using calculated stresses. The stresses can be handled as were the displacements, by comparing with the stress singularity equations [42]. Since stresses are less accurate than displacements for codes using the method of direct stiffness, this approach suffers an additional source of error [46]. This method and the displacement method, however, are

theoretically applicable to three dimensional problems.

Another approach using conventional finite element codes employs line integrals such as Rices's J integral [47]. This line integral is

$$J = \int_\Gamma (Wdy - T_i \frac{\partial u_i}{\partial x} ds) \tag{4}$$

where Γ is an arbitrary contour surrounding the crack tip, W is the strain energy density, T_i are the surface tractions, the u_i are the displacements, and ds is an element of the arc length along Γ. This expression can also be related to the stress intensity factors for plane strain problems by

$$J = (1 - \nu^2)(K_I^2 + K_{II}^2)/E \tag{5}$$

where E is Young's modulus. This approach does not require as fine a mesh as the previous methods, but the contour must be adjusted to minimize the error [46]. The integral is theoretically independent of contour path but is path dependent in practice. The method also suffers in that only one mode of fracture can be analyzed at one time, and the crack surfaces can not be loaded [43,48,49].

Another contour integral has been developed which can solve combined Mode I and II problems (where both K_I and K_{II} are calculated), even for anisotropic solids [50]. Using a form of Betti's reciprocal work relation and comparing contours, a path independent integral can be derived that is fairly accurate.

A different approach to fracture problems using finite elements is based on the strain energy release rate, G, where

$$G = \frac{dW}{dA} \tag{6}$$

which is the change in strain energy dW for a change in crack surface area dA. This quantity can be related to other common terms as

$$G = J = (1-\nu^2)(K_I{}^2 + K_{II}{}^2)/E \tag{7}$$

for plane strain and more generally as [30]

$$G = (1-\nu^2)(K_I{}^2 + K_{II}{}^2 + \frac{K_{III}{}^2}{(1-\nu)})/E \tag{8}$$

By obtaining two finite element solutions of the same body with two slightly different crack lengths, G can be calculated. This method has been sucessfully developed and used by many researchers [51-54]. Good accuracy may be realized with course meshes. This is due to the accuracy of the finite element method in calculating strain energy and the cancelling of errors when taking the difference in strain energy for two different lengths of colinear cracks. In order for the errors to cancel, the local mesh must be identical for both problems. As with the J-integral, this approach permits the determination of individual stress intensity factors when only one mode exists.

Another strain energy approach is to relate it to the rate of change of structural compliance, C, or the inverse spring constant, with crack extension [55]:

$$G = \frac{P^2}{2} \frac{dC}{dA} \tag{9}$$

where P is the applied load. Pook and Dixon [55] calculated the compliance of a cracked body for a number of crack lengths by the use of finite

element codes and then used (9) to calculate G. This approach is comparable to the previous one, but the strain energy is now calculated as one-half the summation of the product of applied forces times their respective change in displacements. The accuracy is good, but, again, only one mode at a time can be analyzed for K.

Since the form of the elastic crack tip singularity is known through equations (1-3), special crack tip elements may be constructed which have the singularity condition built into the local displacement pattern. Use of such an element eliminates a need for fine meshes near the crack tip and avoids the questionable convergence of the finite element method at the crack tip. There are many such methods presented in the literature and they can be divided into special elements surrounding the crack tip, special elements connecting at the crack tip, or modified conventional elements.

The elements of the first type were developed initially by Wilson [56] and by Hilton [57], where displacements generated from William's displacement equations [31] were used as boundary conditions for conventional elements. These fracture elements which are circular, contain a centered crack tip extending radially to the outer edge. Wilson's element is for Mode III problems and Hilton's for Mode I. The displacements in the elements are exact as r→0, thus a balance must be achieved between the abilities of the special elements and conventional elements to model the overall displacement field. Wilson extended his work to plane problems [46,58] including higher order terms in the displacement equations, with some improvement in accuracy. Byskov [59] has a similar triangular element based on

displacements derived from the complex stress function of Muskhelishvili. In all the above elements, there is no compatibility between the singularity elements and conventional elements along their common sides. Wilson's element can have an increasing number of conventional elements, leading to a pseudo-convergence, but Byskov's element is coupled with only three constant strain triangular elements [46]. Others have also developed similar approaches using multiple special regions [60,61].

Tong et al. [62] have derived a crack tip element based on the hybrid element concept that is compatible with conventional elements [63]. Using assumed stress distributions based on the $r^{-1/2}$ type stress field, a stiffness matrix was derived for an octagonal element (may be rectangular). Linear displacement is assumed at the boundary so that the resulting displacements will then be compatible with the displacements from conventional elements at their common sides. Due to the nature of the derivation, the stress intensity factors are an immediate result. This element, for Mode I and II, is readily used with coarse meshes and is easily implemented with other finite element codes [64]. Others have also implemented similar procedures to derive other elements [65,66].

Researchers have also developed triangular elements connecting at the crack tip, notably Wilson [58] and Tracey [67]. These elements have a series of triangles centered at a crack tip much like a cut up pie. In Wilson's formulation, the displacements vary linearly with respect to the angle about the crack tip and are proportional to the square root of the radius. Displacement is continuous at the

interface of the crack elements but are continuous with the conventional
elements at only the nodes. This lack of compatibility occurs because
the displacements on the radial side of the crack tip element do not
vary in the same way as with conventional elements. As more elements
are used in the overall singular crack tip element, the displacement
over the radial edge of the element approaches a linear relation and
continuity with surrounding elements is approached. Tracey's element
allows the displacements to vary linearly at the radial edge assuring
continuity with the conventional elements. Neither formulation is
easily implemented.

The third approach to modeling stress singularities is to modify
existing finite elements close to the crack tip. A recent method
utilizes quadratic isoparametric elements. The modified element's
midside nodes on the sides near the crack tip are moved to the quarter
points near the crack tip [68-70]. The moving of the node causes a
singularity in the form of $r^{-1/2}$ at the crack tip node for strains,
thus a special element is formed. Either the strain energy release
method or the displacement technique can then be used to calculate
the stress intensity factors. This method seems to be easily used
and fairly accurate, but is not quite as good as hybrid elements [67].
Three dimensional possibilities are also being investigated [71].

There are also a large number of other modified finite element
techniques. Some are based on Buekner's weighting functions [72,73],
others use transition functions [74], substructuring techniques
[75,76], or elements with artificially low moduli [77]. Plasticity
effects have been considered [57,78] and anisotropic fracture is

being investigated by finite element techniques [79-81].

The previous discussion covered the analysis of stationary cracks.
Also of great interest is the criterion for initiation of crack growth
and the direction of propagation.

Mixed Mode Fracture Mechanics

According to Griffith, "the crack will grow in the direction along
which the elastic energy release per unit crack extension will be
maximum and the crack will start to grow when this energy reaches to
a critical value" [82].   At first, analytical complexities prevented
the analysis of non-colinear crack extension problems, so only simple
Mode I problems were investigated. Since real structural problems
often involve combinations of two or three modes, one must be able to
account for the situation in which the crack growth direction is not
in the original plane of the crack. A summary of the various mixed
mode criteria will be presented here.

One of the first studies in this area was conducted by Erdogan and
Sih [82] in the investigation of non-colinear crack growth in two-
dimensional geometries. The investigation supported a criterion stating
that:

1) Crack extension starts at its tip in a radial direction

2) Crack extension starts in a plane perpendicular to the direc-
   tion of greatest local tension.

Using the singular portion of the equations described earlier for the
stresses at a crack tip, but in polar coordinates,

$$\sigma_{rr} = (2\pi r)^{-1/2} \cos \frac{\theta}{2} \left[K_I (1 + \sin^2 \frac{\theta}{2}) \right.$$

$$\left. + \frac{3}{2} K_{II} \sin\theta - 2K_{II} \tan \frac{\theta}{2} \right] + \ldots$$

$$\sigma_{\theta\theta} = (2\pi r)^{-1/2} \cos \frac{\theta}{2} \left[K_I \cos^2 \frac{\theta}{2} - \frac{3}{2} K_{II} \sin\theta \right] + \ldots \tag{10}$$

$$\tau_{r\theta} = \frac{(2\pi r)^{-1/2}}{2} \cos \frac{\theta}{2} \left[K_1 \sin\theta + K_2 (3 \cos\theta - 1) \right] + \ldots$$

the angle of propagation can be found by maximizing $\sigma_{\theta\theta}$ with respect to θ as in

$$(2\pi r)^{1/2} \frac{\partial \sigma_{\theta\theta}}{\partial \theta} = 0 \tag{11}$$

where r is factored out of the equation. This results in

$$\cos \frac{\theta}{2} \left[K_I \sin\theta + K_{II} (3\cos\theta - 1) \right] = 0 \tag{12}$$

which gives

$$\theta = \pm \pi$$

and

$$K_I \sin \theta + K_{II} (3 \cos \theta - 1) = 0 \tag{13}$$

as solutions. The first solution corresponds to the free surface conditions of the crack and is discarded; (13) yields the maximum $\sigma_{\theta\theta}$. Knowing the particular stress intensity factors of the problems, prior to growth, the crack trajectory can be determined. This criterion was

compared to experiments conducted with plexiglas sheets with various crack geometries and loading conditions. Most widely used was a large sheet containing a centered crack inclined to the uniform tension at the edge of the sheet. The results compared fairly well with the trajectory criteria, allowing for the large amount of data scatter. An important comment was made [81] in that the greatest energy release occurs when the crack propagates approximately perpendicular to the direction of maximum tension, indicating another possible criterion.

The same problem was reinvestigated by J.G. Williams and P.D. Ewing [83] with a slightly improved criterion. Inclusion of the next higher order term in the equation for $\sigma_{\theta\theta}$ improved correlation with the previous experimental evidence and also with new data gathered by the investigators. Again a large amount of data scatter was present and the same inclined crack geometry with plexiglas was tested. A correction was made by Finnie and Saith [84] to the equations Williams and Ewing used which also improved correlation with data. The added term approach has forced the necessity of evaluating the expressions at a certain critical value of the radial distance from the tip, r, while previously r had been factored out as in equation (11). The value of r is then adjusted to fit experimental data. In further comments, Williams and Ewing pointed out that even higher order terms may be needed for bending experiments [85]. This was followed up with tension and bending tests with inclined edge cracks and comparison with the higher order term approach met with some success [86]. For completeness, Sih and Kipp [87] conducted an analysis examining the stresses found from the exact solution computed from a degenerate elliptical

cavity. The use of these equations is also dependent on evaluation
with a certain value of r. This criterion compared with experimental
data with about the same success as the previous studies [87]. Some
of these maximum stress criteria are presented in Figure 3 for only
one value of r.

A minimum strain energy criterion has been proposed by Sih
[87-90]. The work is an extension of some ideas presented earlier
[82]. The change in strain energy density with polar angle at the
crack tip was derived as a homogeneous quadratic form of K_I and K_{II}.
This new criterion is specified as follows:

1) The crack will propagate in the direction of minimum strain
   energy density at the crack tip

2) The onset of growth will be controlled by a critical value
   of the minimum strain energy density.

Using only the singular portion of the stress equations (1-3),
the strain energy density of a infinitesimal cube is calculated,
resulting in:

$$\frac{dW}{dV} = \frac{1}{r\pi^2} (a_{11} K_I^2 + 2 a_{12} K_I K_{II} + a_{22} K_{II}^2 + a_{33} K_{III}^2) \quad (14)$$

where the coefficients a_{ij} are functions of the polar angle about the
crack tip, Young's modulus and Poisson's ratio. This three dimensional
criterion is written as:

$$S = \frac{1}{\pi^2} (a_{11} K_I^2 + 2 a_{12} K_I K_{II} + a_{22} K_{II}^2 + a_{33} K_{III}^2) \quad (15)$$

where S is proportional to the strain energy density. This equation
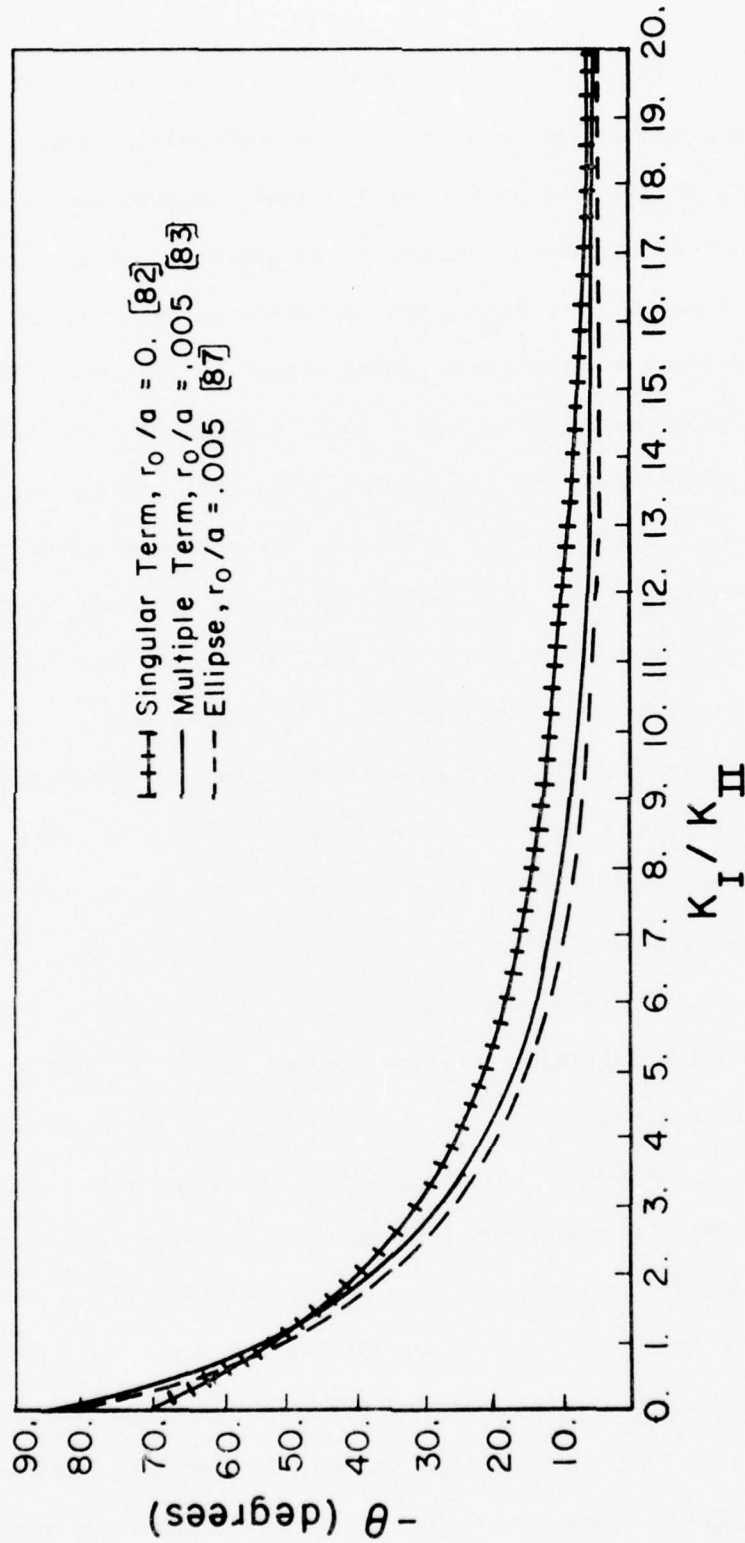is examined to find its minimum with respect to the polar angle and the

Figure 3. Crack propagation angle vs stress intensity factor ratio for various maximum stress criteria.

value of the angle producing the minimum is the direction of propagation.

This criterion has been compared with experimental evidence in tension and compression [86,90-92] and has been found to have little improvement over the previous maximum stress approach. The S criterion has been questioned for its dependence on Poisson's ratio, ν; it has failed to predict accurately crack growth direction in cross-rolled beryllium where the value of Poisson's ratio approached zero [91]. In this case, the maximum stress criterion was significantly better. The minimum strain energy density criterion has also shown poor correlation with cone fractures in fused silica where the material is nearly incompressible ($\nu=.5$) [92]. It also has not been proven that the critical value of S is a material constant as it should be [90].

In order to improve the correlation with data, a more general and physically realistic model has been proposed by Sih [87,89,93]. The crack is approximated by a narrow ellipse. The exact energy density based on linear elastic theory is calculated with the complete series expansion of the stresses about the ellipse crack tip [87]. This modified criterion is then dependent upon the radius of curvature of the ellipse, ρ, and the distance from the crack tip at which the modified S is evaluated. Sih explains that this critical value of r depends on the crack geometry and loading [89]. By adjusting ρ and r, Sih has demonstrated improved correlation with data [87,92].

Francis and Ko [94] have examined the minimum strain energy density criterion in terms of the stresses about an elliptical crack. They derived three forms based on the use of plane strain, plane stress, and deviatoric plane stress equations. As shown in Figure 4, for one
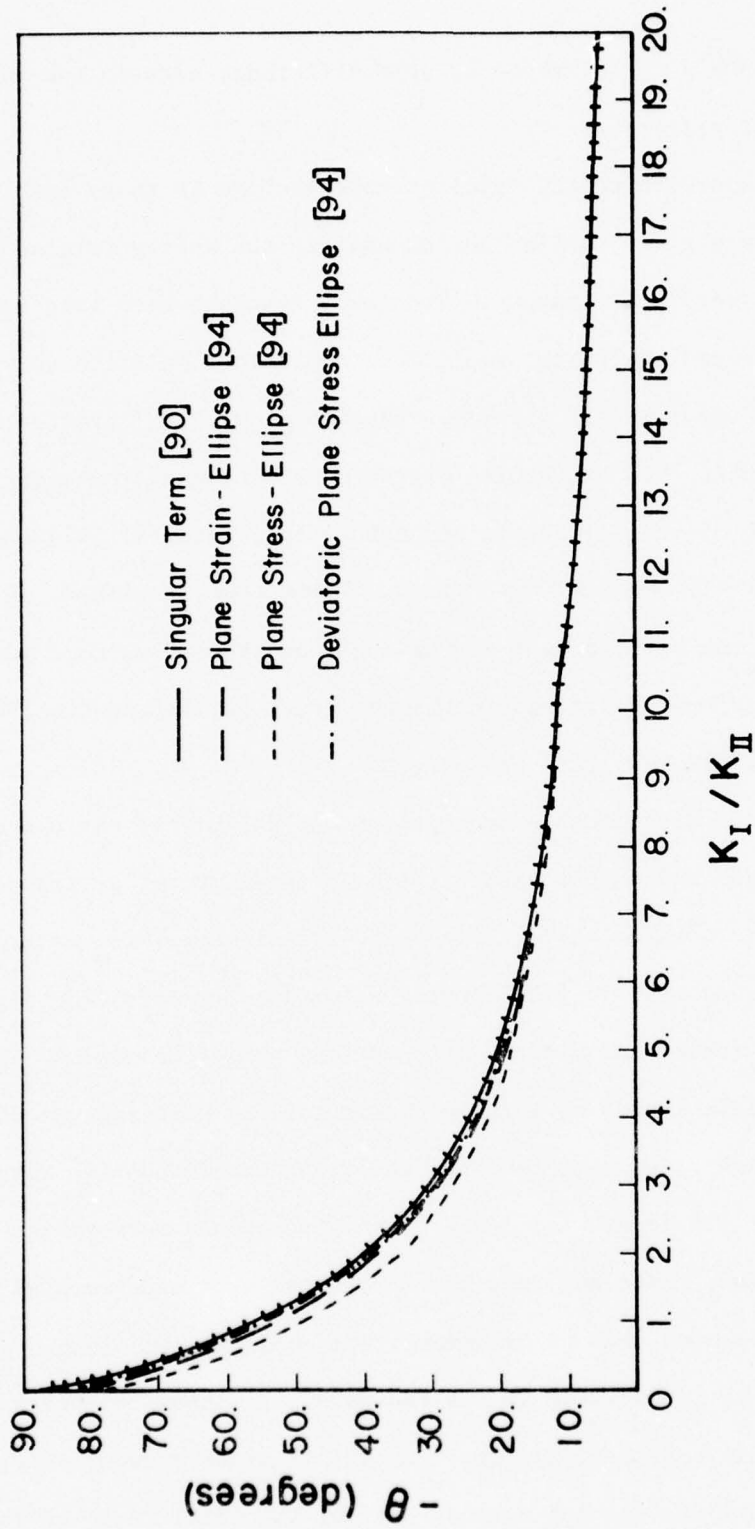
Figure 4. Crack propagation angle vs stress intensity factor ratio for various minimum strain energy density criteria evaluated for $\nu = .3$.

value of Poisson's ratio, there is some difference between the various forms of the S criterion.

Another approach to the combined mode problem is to go back to Griffith's quote given earlier and to analyze the energy release as a crack grows a very small amount. Two investigations have been made using the advanced analytical tools developed since Griffith to examine the combined Mode I and II problem. Hussain et al. [95] started with a line crack which has an angular extension at one end. Considering a virtual growth of this extension and using the J-integral [47] and equating the integral to strain energy release rate, a maximum of the release was found with respect to the angle of the extension. The authors use various analytical techniques, such as mapping functions, complex potentials and limit procedures.

Due to some questionable assumptions and failure to conform with the known stress and displacement fields in the limit of a straight crack that were pointed out by Knauss and Palaniswamy [92], an improved analysis was conducted in [92]. Using a complex potential for the stress analysis of a crack, and a crack with various angled increments at one end, the strain energies of various configurations were evaluated. Then the release rate was calculated and a maximum found with respect to the angle. The length and angle of the increments were varied to find the maximum. This analysis was correlated with experimental evidence with a good deal of agreement [92]; however, the length of the increment had to be adjusted to fit the data. The physical basis for using other than a vanishingly small amount of crack growth is not clear. The analysis was not carried out for the total range of the

problem, leaving undone the important case where shear predominates in the combined problem; see Figure 19. These maximum energy release criteria are compared in Figure 5.

Other researchers have used finite element codes to examine the combined mode problem. These have followed the maximum strain energy release rate and maximum stress criteria for plane fracture problems. Coughlan and Barr analyzed the infinite sheet-inclined crack problem using the energy release criterion [96] and found results that fall between the maximum stress criterion and the strain energy density criterion. As seen in Figure 5 the results agree well with the maximum energy release rate criterion in some portions of the plot. Unfortunately, the finite element analysis was also not followed through in problems where large amounts of shear are present. Marinshaw and Lindsey [97] performed an investigation of the edge-notched biaxial strip with experiments with solid rocket propellant and case liner materials. Predictions were made of the crack angle using a finite element code to calculate the maximum normal stresses about the crack tip. Incorrect propagation angles were predicted by the classical sharp tip solutions of linear theory and finite elements, due at least in part to the blunt nature of the actual tip. Use of an artificially blunt crack tip in the finite element analysis produced a favorable correlation. It may be conjectured that stress equations for ellipses could provide equally good correlation. Helen and Blackburn [98] have also conducted a finite element investigation using the energy release rate method. Their results are very poor for cases where shear is more significant than tension [98].
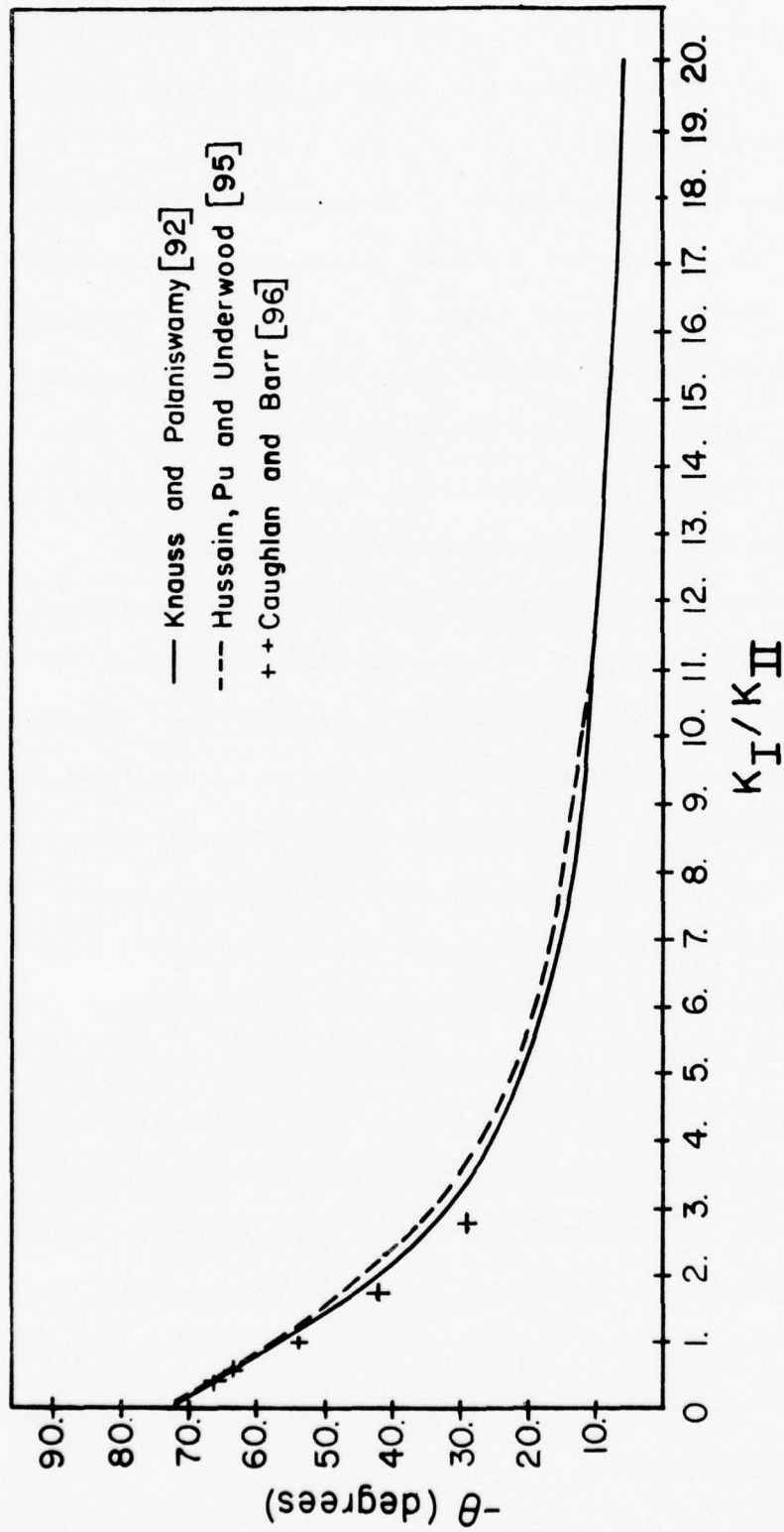
Figure 5. Crack propagation angle vs stress intensity factor ratio for various energy release rate criteria.

Other analyses are being proposed for mixed mode fracture mechanics.
Bilby and Cardew have [99] developed a theory comparing the stress
intensity factors at both the initial crack tip and the incremented
crack tip by means of quadratures [100]. This three-dimensional
formulation compares well in the two dimensional case with certain
experimental data [99]. Morozov and Fridman [101] have made a suggestion
that cracks generate and propagate along a geodesic line (shortest
distance between two points on a surface) passing through the point
of initiation. An approximate variational scheme was proposed based
on the minimization of the difference between the surface energy and
the strain energy of the body. Lindsay [102] has proposed a hybrid
criterion using the crack growth orientation as found from the maximum
stress criterion and a failure law based on the stress invariants near
the crack tip.

On the basis of the literature review, it is the belief of this
author that, for sufficiently small regions of nonlinearity at the
crack tip, the maximum energy release rate theory governs crack
growth at all stages of growth. The maximum stress criterion represents
an approximation which improves as the crack propagates and aligns
itself perpendicular to the greatest tension. An attempt was
made to prove that the two criteria are equivalent [103].

For solving engineering problems, a surface relating the stress
intensity factors (K_I, K_{II}, K_{III}) can serve as an initiation cri-
terion. Figure 6 shows such a criterion for two dimensional problems
[82, 88, 94, 95]. The energy release rate criterion fits experi-
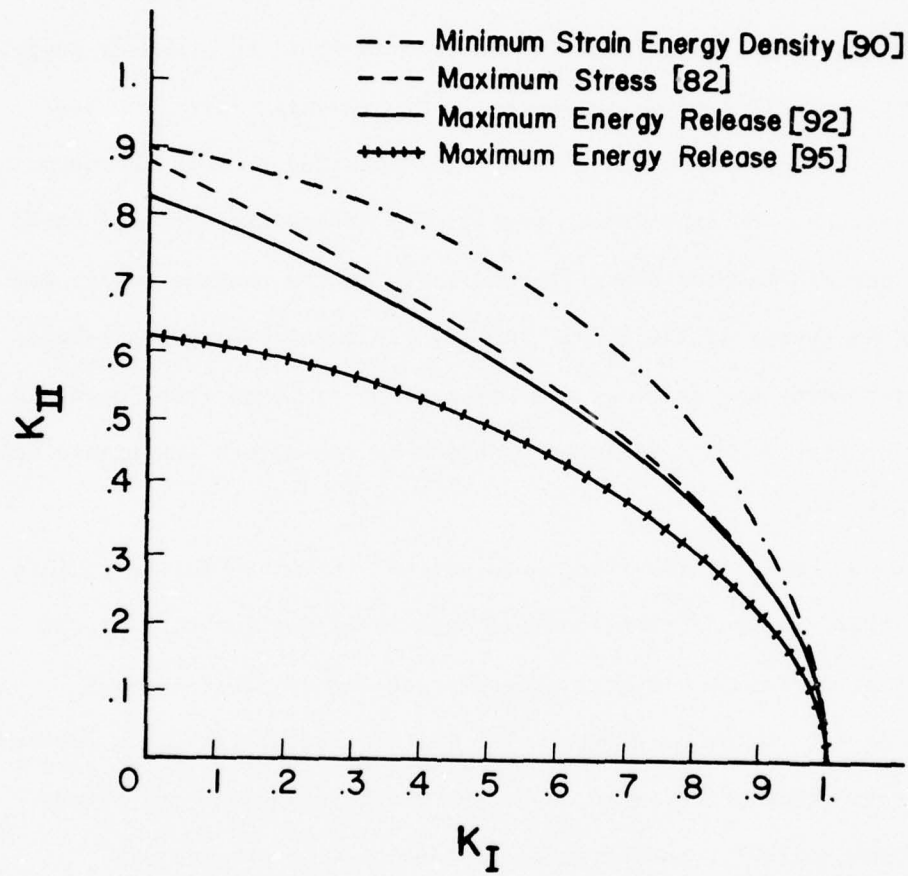mental data quite well as shown in a later section of this paper.

Figure 6. Interaction of K_I and K_{II} for various criteria.

However, it still remains to calculate the energy release rate for the complex three dimensional problem.

FRACTURE TESTS

Motivation

An experimental program was designed to provide fracture data to investigate the nature of crack growth between fibers in a composite material. This data was also to be compared to predictions made by the various crack trajectory theories to see which criterion fit the experimental data best. Thus the experimental model should be indicative of a cracked matrix restrained by relatively rigid fibers and should be a new test of combined mode fracture theories. While microcracks in composites are truly three dimensional, a biaxial strip with initial cracks parallel to the long sides was considered to be a suitable model to begin investigation of microcracking phenomena.

Material Selection

The microcracking behavior described earlier is found in most common fiber reinforced composites: graphite or glass fibers in a plastic matrix. These plastics usually are epoxy systems that have been especially formulated for use in composites [1,2].

In the interests of being able to compare data with the literature and ease in use, plexiglas was employed instead of an epoxy. Overall mechanical properties of the two materials are quite similar [104,105]. The fracture behavior could also be expected to be similar even in the matter of crazing [106-113] (crazing is the lessening in density due to microvoid growth, usually found around a crack tip). After surveying the literature, it was concluded that crazing or ductility might be a factor in determining the overall fracture direction [114-115]. Therefore, in order to compare

experimental evidence on a new geometry with the wealth of data generated with plexiglas [82,83,85,86] the same material was chosen. The ease in producing readily visible cracks was also an important factor in choosing plexiglas.

Samples and Equipment

GM grade plexiglas sheets as specified by the Rohm and Haas Company [117] were ordered in three nominal thicknesses (0.03, 0.06, 0.125 inches). All the sheets needed were ordered at one time to reduce any batch variability. The material was stored in an area where the temperature and humidity were the same as the testing area (75°F at 50% relative humidity).

The sheets, which arrived with protective masking tape, were prepared for a cutting to the required dimensions, by drawing the sample's dimensions directly on the tape. All sample dimensions were drawn slightly oversize to allow for final trimming. To compensate for any induced anisotropy caused by manufacturing, half of the samples of one sheet were cut perpendicular to the other half. Using a tungsten carbide band saw blade, with a slow feed rate and band saw speed, the samples were rough cut from all the sheets. After removing the tape, several coupons were mounted in a vertical mill at one time and machined to the final dimensions using a fly cutter tool. Inspection of the edges showed little damage if care was taken to prevent the samples from vibrating. The thinnest sheets (0.03 inches) showed a tendency to edge crack upon cutting; samples with edge cracks were rejected.

Constant crosshead rate tests were conducted using a few special samples taken randomly from the three sized sheets. These samples

(10 x 1.25 inches) were cut as the above. Micro-measurements' strain
gages, type EA-06-125BZ-350, were bonded to the sample's center both
along the axis and perpendicular to the axis of the sample. Mirror
image gages were applied to the opposite side of the coupon. Micro-
measurements' M-bond AE-15 adhesive was used and the gage-adhesive
was cured under slight pressure for four hours at 140°F, well below
any temperature that could cause permanent dimensional, physical or
chemical changes to this material. Strain gage measurements were
recorded using a B&F Instruments' Strain Gage Acquisition System and
a modified Hewlett-Packard 561 Digital Printer. This system operated
at the rate of two channels per second, with capability up to ten
channels of strain gage signal conditioning with wire length compen-
sation.

The samples were placed with their greatest length in the loading
direction and clamped in the standard wedge-action grips of the constant
crosshead rate Instron Testing Machine. Using a rate of 0.02 inches/
minute and at the temperature and humidity described previously (slight
variations in these conditions were recorded) the samples were pulled
apart until sudden failure occured at the center, under the strain
gages. During the test the applied crosshead displacement, resulting
load, the two axial strains (both sides) and the transverse strains
(both sides) were recorded.

In reducing this data, the opposing strains were averaged. The
transverse strains were adjusted for transverse wire effects in the
gages due to the applied displacement, by equations provided by Micro-
measurements [118]. Using the stress (the resultant load/original area)

and the strain (averaged axial) from these tests, a stress/strain curve was plotted. This is shown in Figure 7. The stress/strain curve is linear below the level of applied stresses used in the other experimental work. The calculated Young's Modulus (σ/ε at a point) was 433,000 psi, comparable to the manufacturer's value of 450,000 psi. The Poisson's ratio was found to agree with the manufacturer's value of 0.35. The calculated values were used in the work in this report.

With these preliminary tests completed, a review of the litera-ture [119-122] led to the biaxial strip size of 8 x 1 inches; these dimensions would cause an intial crack to be in the biaxial stress field (far enough from the ends of the strip). The samples were cut in the same manner as the previous discussion. Based on Mueller's work [121] crack lengths of one and one-half inches were decided upon; this would let the test configuration approach the geometry of a crack in an infinite strip.

The cracks were cut parallel to the long sides of the strips, as in Figure 8. An initial crack or slit was machined with the use of a very fine circular saw blade mounted in a vertical mill. The resulting slit was nominally 0.005 inches thick. This machining produced a fine slit with a small curvature at each end, the curvature being more pronounced with the thicker samples. (Due to the circular nature of the blade and mounting of it, the slit could not have ends perpendicular to the faces of the sheet). A natural crack tip was formed by first applying in-plane compression on the long sides of the strip ahead of the crack (with a vise) and second by wedging open
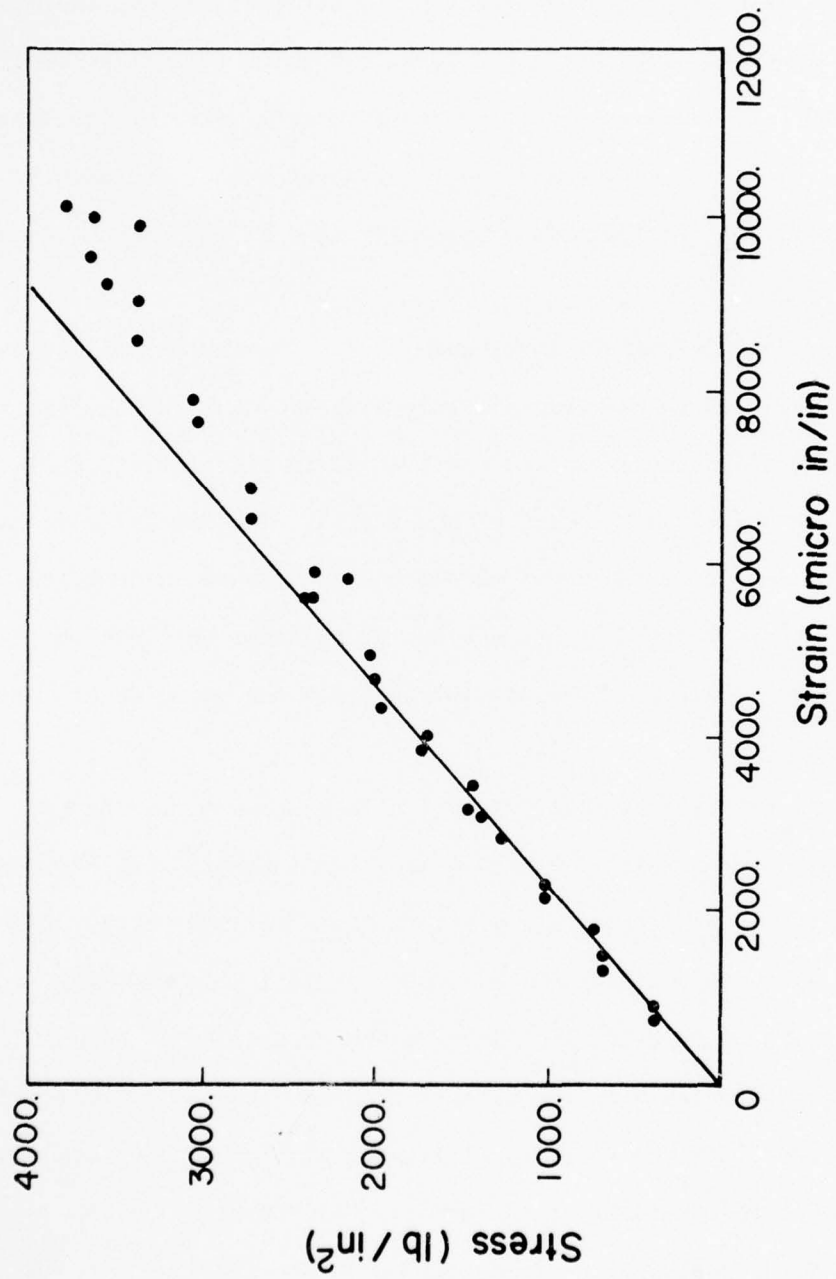
Figure 7. Stress/strain curve for plexiglas used in experiments.
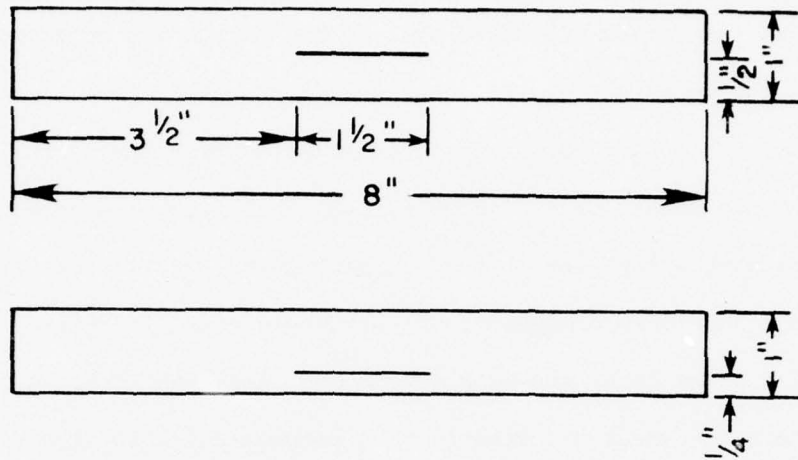
Figure 8. Center crack and off-center crack biaxial
strip geometry.

the crack (with a razor blade) to produce controllable colinear crack growth. This extension was for a distance greater than the sheet thickness. This crack tip had to be perpendicular to both sheet faces as examined by the naked eye, or the sample was rejected. The process was repeated for the other end of the slit.

The test apparatus was designed so as to test the strips in tension, simple shear, or in a combination of the two. As seen in Figure 9 two plastic strips were bonded perpendicular to stainless steel bars. The steel bars were designed to be extremely rigid in respect to the plexiglas. The outer two bars were wider than the inner bar to facilitate the shear experiment. The perpendicular bonding was assured by a special bonding fixture as seen in Figure 10. The bar was placed in the bottom of the fixture, and the inner moveable plates supported the plastic perpendicular to the bar. With the use of a micrometer, the moveable plates were adjusted until the biaxial strip was centered perpendicular to the bar. The moveable plates were locked into place, the two sides of the fixture loosened, the biaxial strip removed, adhesive applied, the system reassembled and left until bonding was complete.

Two strips of identical dimensions were bonded to two bars and then the bars placed so as to have the strips parallel to the table's surface. The smaller middle bar was placed at a measured height above the table so as to have the bonded strip's free edge perpendicular to the middle bar's surfaces. Use of an angled square aligned the three bars, adhesive was applied and the two free edges of the strips were bonded to opposite sides of the middle bar. After initial cure, the holding plate, as seen in Figure 9, was fixed to the
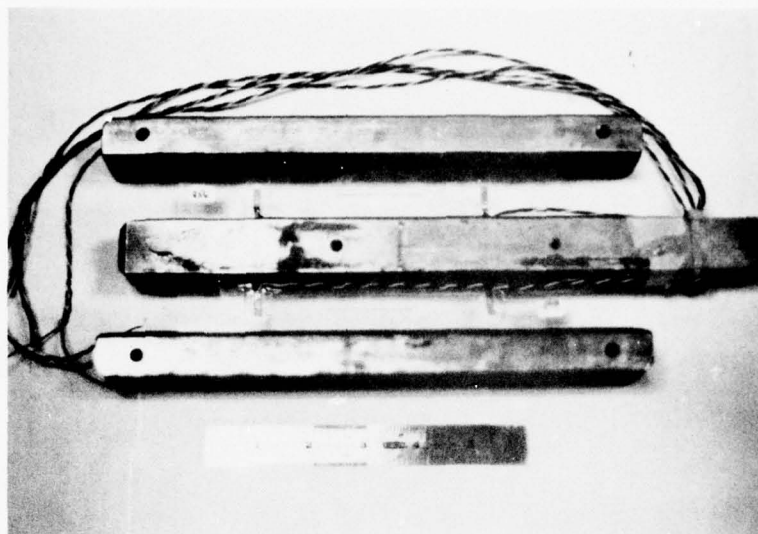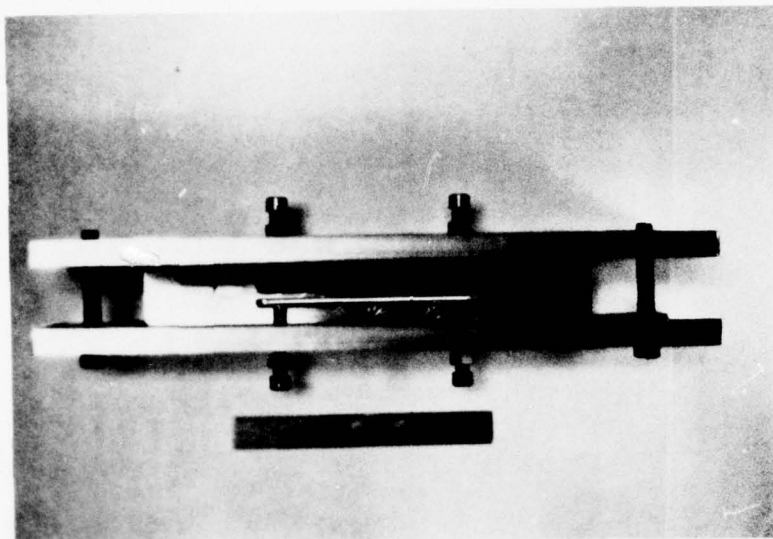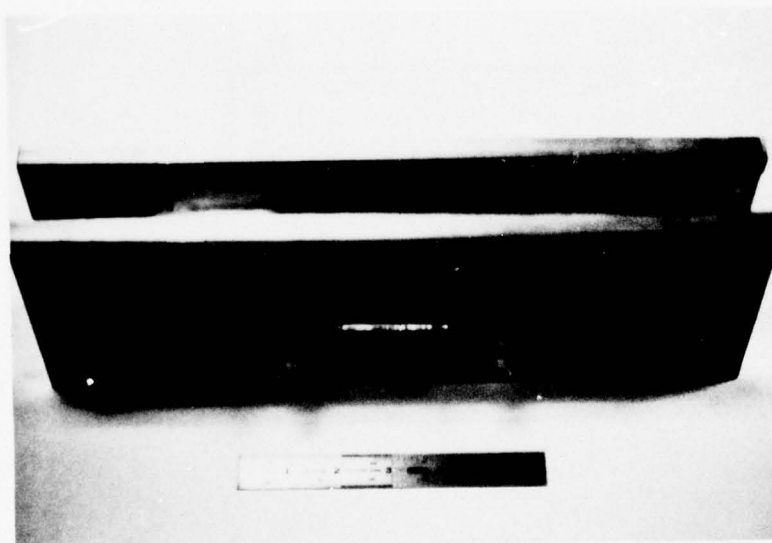
(a)
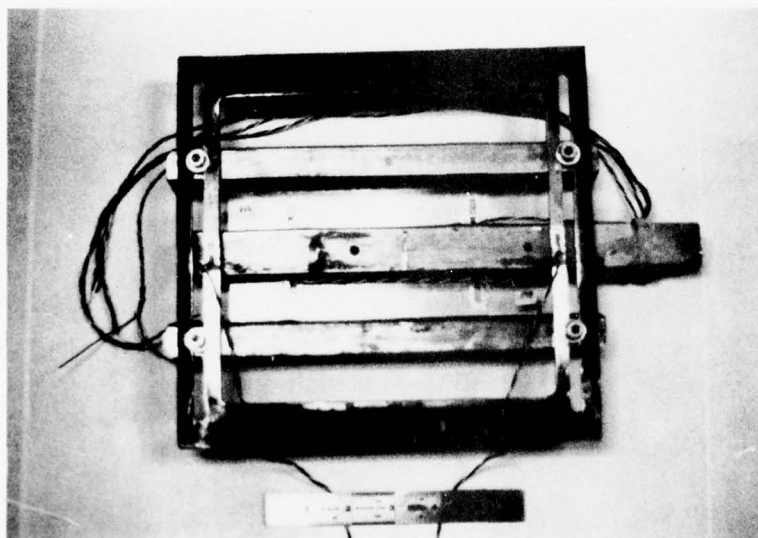
(b)

Figure 9. Dual bonded test system without (a) and with (b)
holding plate, used in bonding and testing specimens.

(a)

(b)

Figure 10.   Top (a) and side (b) views of bonding jig.

system to prevent movement and the whole assembly was cured at 140°F
in a large walk-in environmental room located in Texas A&M University's
McNew Laboratory.

Loading fixtures were designed so as to hold the sample system
and be compatible with the Instron Machine. As in Figure 11, the
samples could be pulled in tension or shear. The tension was applied
through both the samples at one time. The samples were pulled in
simple shear in this so-called double lap shear test (i.e. the middle
bar stays fixed and the two outer bars move up). In order to perform
a combination of tension and shear, the sample system was pulled to
the desired tension level, the holding plates were lightly screwed into
the outer bars, C-clamps were applied to prevent rotation of the plates
upon tightening, and the plates were tightened with the use of wrenches.
Two holding plates were used, one for each side, and were designed to
hold the system rigidly in all shear tests, with or without pretension.
The tensioned sample system was removed from the Instron and the load-
ing fixture rotated 90°. With the holding plates, the outer two bars
remain parallel to each other when the outer bars are pulled upwards.
Figure 11 shows the described apparatus without the plates to allow easy
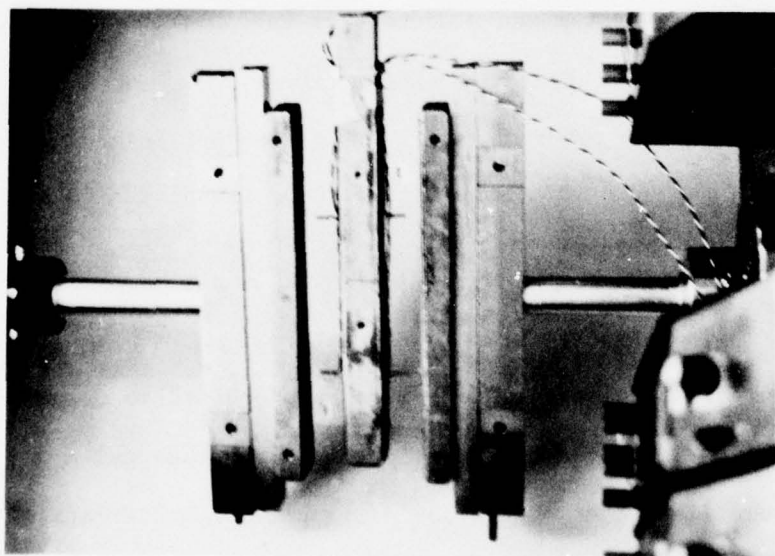inspection for the reader.

Experimental Considerations

In any experimental effort care must be exercised to insure that
the intended experimental model and the actual experimental model are
the same. Sometimes, due to physical difficulties, modifications to
the model must be made and then corrected for.
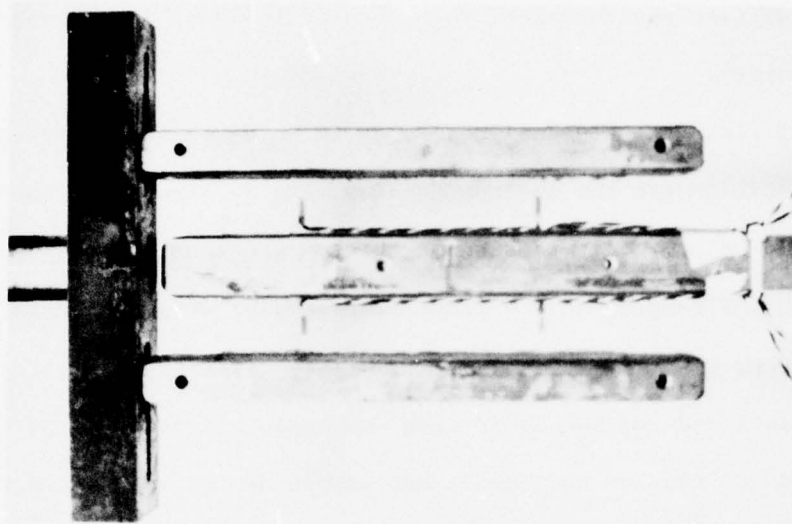
(b)

(a)

Figure 11. Sample system shown in tension (a) and shear (b).

The bonding of plexiglas to stainless steel was no easy matter. The two dissimilar materials could be bonded together with various adhesive systems, but the high stress concentrations at the corners of the strip caused premature failure. This problem was eliminated by bonding 0.06 inch thick plexiglas plates to the surfaces of the stainless steel bars with an epoxy system. This epoxy consisted of 40% Versamid 125 hardener and 60% R-815 resin (by volume) as supplied by the King Chemical Company. This system was cured for 24 hours at room temperature. The plexiglas surfaces and edges were roughened for bonding using grade 200 silicon paper and cleaned with acetone, M-Prep Conditioner A and B were used, then Freon TF was sprayed on and wiped clean with tissue. These materials were obtained from Micro-measurements. With these clean surfaces and edges, the biaxial strips were then bonded perpendicular to the plexiglas plates with the use of Daybond Thickened Cement manufactured by Dayton Plastics Inc. This allowed the bonding to be essentially cohesive due to the nature of the cement and to have no excess that would mar the orthogonal arrangement of plate and strip. Then elevated temperature was used for curing, as described earlier, for at least three hours.

The elevated temperature (at approximately 140°F) was low enough to prevent any permanent damage to the samples such as the dimensional changes at high temperature predicted by the manufacturer of the GM plexiglas used. The material at 140°F was well below the glass transition temperature of plexiglas, nominally 220°F. This temperature is defined as the temperature above which the physical mechanisms of deformation within the polymer start to change due to a significant

change in free volume [123]. Since the tests were conducted at 75°F

at 50% relative humidity (the samples were at these conditions for at

least twelve hours, prior to testing) viscoelastic behavior was

negligible. Strain gage heating was neglected since others have found

this to be negligible [10]. Temperature and humidity were recorded

in all tests to check any affects, and none were found. In order to

check for rate dependence, some tests were made at three displacement

rates (0.002, 0.02, 0.2 in/min). Little rate dependence could be

found at these test conditions.

Due to the change in the stress field and boundary conditions

of the biaxial strip because of the addition of the plexiglas plates,

an analysis was undertaken. Viewing the strip and plates as an I-beam,

(seen from the end of the strip) a plane strain finite element analysis

was made. (The program used will be described in a later section).

Checking all conditions where the different strips were greater,

equal to, and smaller in thickness than the pre-bonded plates, we found

by adding approximately one half of each plate thickness to the

strip's height, the correct biaxial stress field was achieved. Thus

the strips' heights were considered to be 1.06 inches.

When conducting any multi-axial loading experiment, proper

alignment is critical. Alignment was kept as correct as possible in

the bonding precedure described earlier. This and the loading align-

ment were checked by a series of tests with strain-gaged sample

systems. The gages described earlier were fixed on both ends of the

strip, one and one-half inches away from the edge (to avoid end

effects) on opposite sides of the strip. The system had four gages,

two to a strip. This can be seen in Figure 11. The gages were moni-
tored with the use of Vishay/Ellis - 10 Portable Strain Indicators.
Very small amounts of bending occurred in loading in tension, which
was eliminated during the placing of holding plates. After taking
the tensioned sample system from the Instron Machine, strains were
still recorded. Less than 5% decay in tensile strain was achieved
if the holding plates were properly fixed. Upon shear loading,
negligible slipping was recorded by the strain indicators.

Tests were made to check how close the man-made cracks resembled
natural flaws. By scribing a plexiglas strip on one side with a tool
and gently tapping the other side with a chisel and hammer, a very
natural crack can be made. Due to the difficulty in producing a number
of these cracks, only a few strips were tested with these flaws.
Little difference could be detected between test results with these
more natural cracks and the machined crack's test results.

Testing

Much of the test procedure has been described already, but a
short unified presentation will be presented here. The strips were
measured with the use of calipers and, as nearly as possible, matched
strips were used together. After bonding to the steel bars, a test
ratio of tension to shear load was decided upon, and the test conducted.
Tension, tension/simple shear and simple shear tests were conducted
with the center crack samples. With the off-center crack samples,
only tension and simple shear tests were made. Table 1 is a summary
of this test program. All the previously described experimental
considerations were taken into account.

Table 1. Summary of Fracture Tests

Fracture Mode	Crack	Sample Thickness (inch)	Number Tested
Opening	Off-centered	0.03	4
		0.06	2
Shearing	Off-centered	0.03	1
		0.06	1
Opening	Centered	0.03	3
		0.06	2
		0.125	2
Shearing	Centered	0.03	3
		0.06	3
		0.125	2
Combined	Centered	0.03	12
		0.06	12
		0.125	2

The samples were pulled to failure and the failure loads (tension, shear, tension and shear) were recorded. Since not all four crack tips initiated at once, four sets of loads resulted. The cracks started quite suddenly, propagated quickly in a defined direction, and stopped at the interface between sheet and strip. Further increases in the applied displacements caused slow propagation down the interface. Little out of plane bending resulted as the crack tips initially propagated; but after much propagation down the interface, bending occured so the tests were halted. Examples of the typical load histories of the tests are shown in Figure 12.

Data Reduction

In order to calculate the correct initial stress intensity factors (at failure), a plane stress finite element analysis was conducted of the biaxial strip. Modeling the strip (3 x 1.06 x 1 inches) was accomplished with cracks of lengths 0.25, 0.50, 0.75, 1.25, 1.50, 2.00, and 4.00 inches in length. (The computer programs used will be described in a later section). The tension test was modeled by displacing rigidly the long edge boundaries perpendicular to the crack (holding displacement parallel to the crack fixed). The simple shear test was modeled by displacing rigidly the long edge boundaries parallel to the crack (holding displacement perpendicular to the crack fixed). These two tests were modeled over the range of crack lengths used. The load for a unit displacement was found in all the cases by integrating the stresses over the boundary. The analysis also confirmed that the strain gages used for checking alignment were correctly placed to avoid end effects. The stress intensity factors were plotted
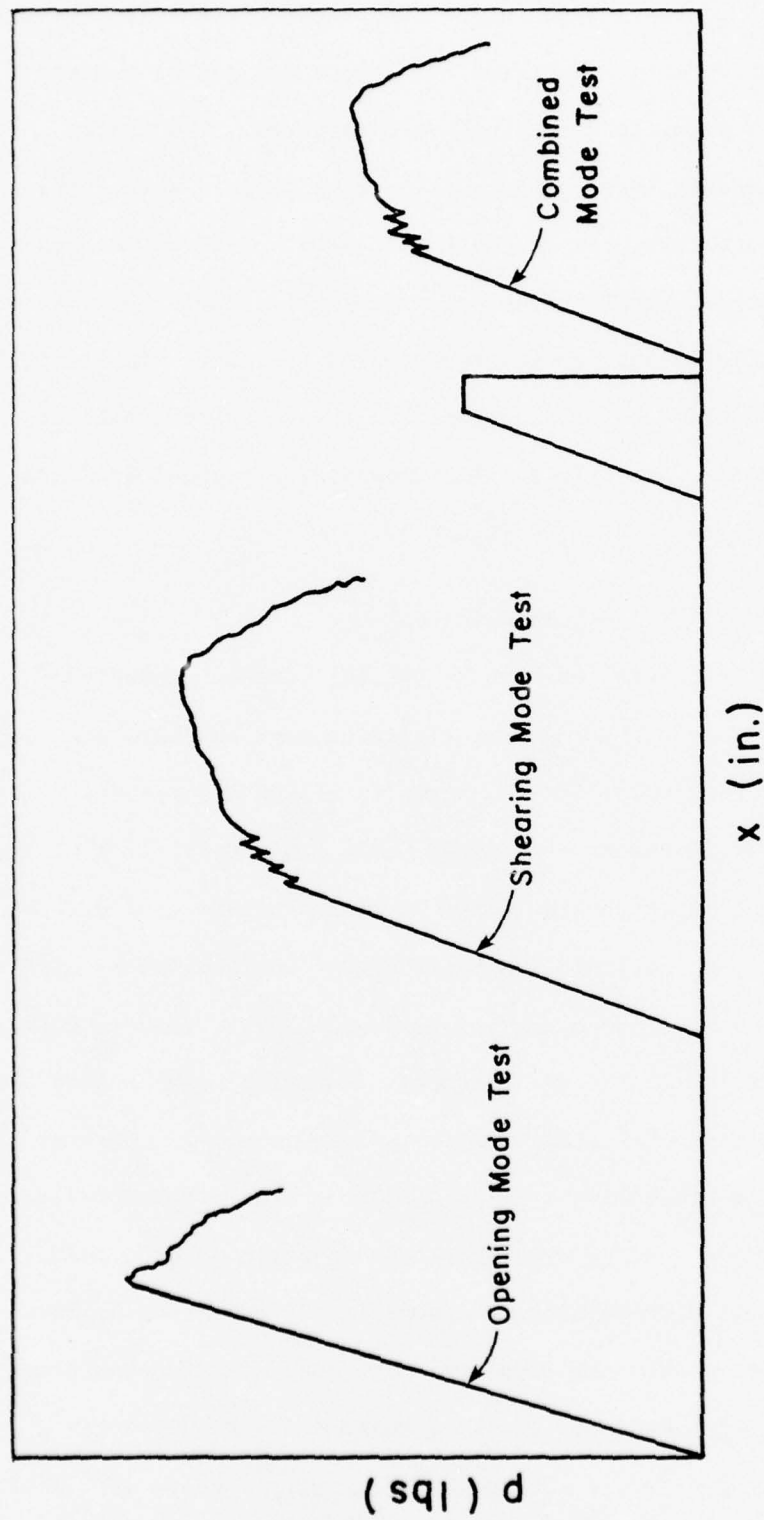
Figure 12. Examples of loading histories (resultant load vs cross-head displacement) used in fracture tests.

versus crack length/strip height as in Figures 13 and 14. The
solid and dashed curves represent equations for a crack in an all-
around infinite sheet (solid line) [36], and a crack in an infinitely
long strip [121]. The finite element results show the close agreement
with theory. The slightly lower values for the stress intensity
factors are believed due to the strip not being infinitely long. The
finite element computed load versus crack length/strip height is
plotted as in Figures 15 and 16. Then the ratio of stress intensity
factor to load was plotted versus crack length/strip height as in
Figures 17 and 18. Using these last figures, knowing the crack length
of the sample, and the loads causing crack growth, the correct stress
intensity factor could be calculated for any amount of grip displacement.

The angles of crack propagation for combined loadings were
initially measured directly from the samples. As this was difficult,
later samples were removed from the bars by a chisel, laid upon paper
and crack path traced. The initial angle of propagation was used for
comparison with theory. It was found that the crack propagated along
a straight line for a significant distance, then curved to meet the
boundary as shown in the section on fractography. This distance decreased
for increased levels of tension in combined mode testing. The angle
between this initially straight line and the crack was used as the
initial propagation angle .

Results

The results were plotted in such a way that they could be compared
easily with the current theories describing crack trajectories.
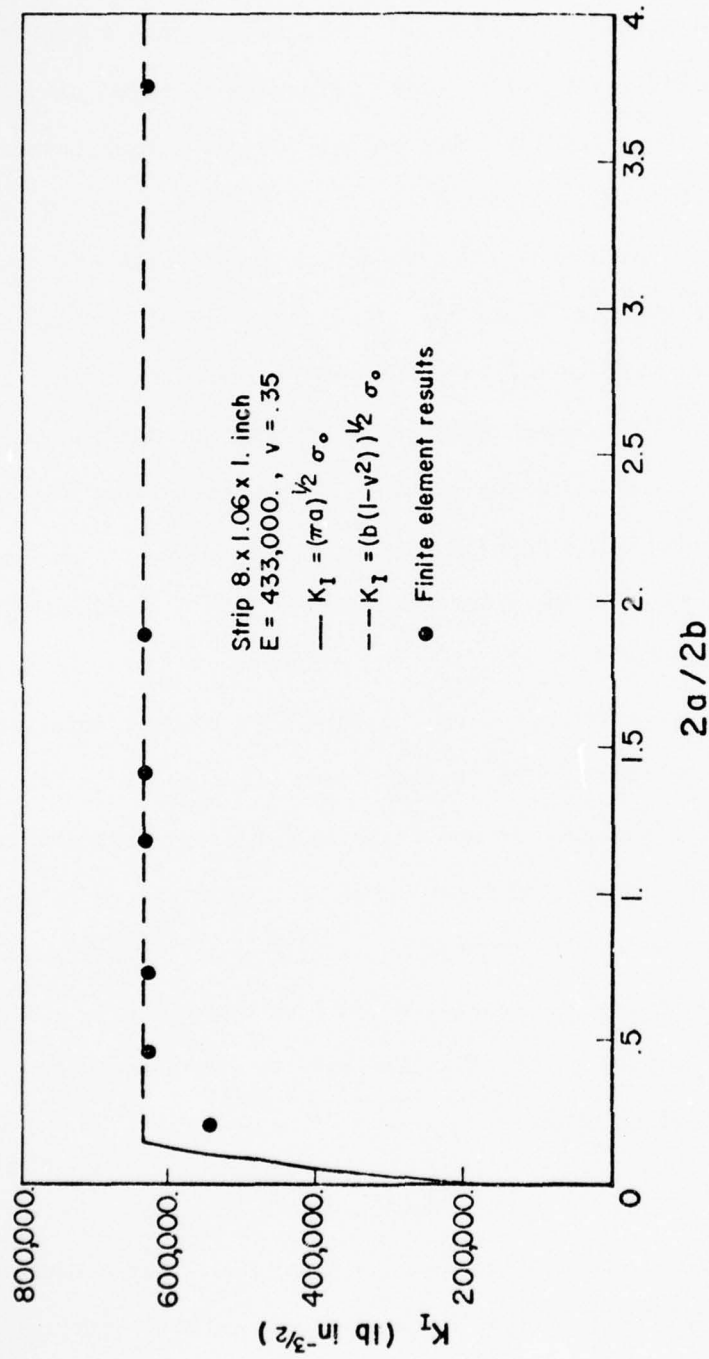Figure 19 shows the ratio of critical stress intensity factors versus

Strip 8. x 1.06 x 1. inch
E = 433,000., v = .35
—— $K_I = (\pi a)^{1/2} \sigma_o$
— — $K_I = (b(1-v^2))^{1/2} \sigma_o$
● Finite element results

$2a / 2b$

K_I (lb in$^{-3/2}$)

800,000.

600,000.

400,000.

200,000.

0   .5   1.   1.5   2.   2.5   3.   3.5   4.

Figure 13. Opening mode stress intensity factor vs crack length/
strip height for unit displacement.

49
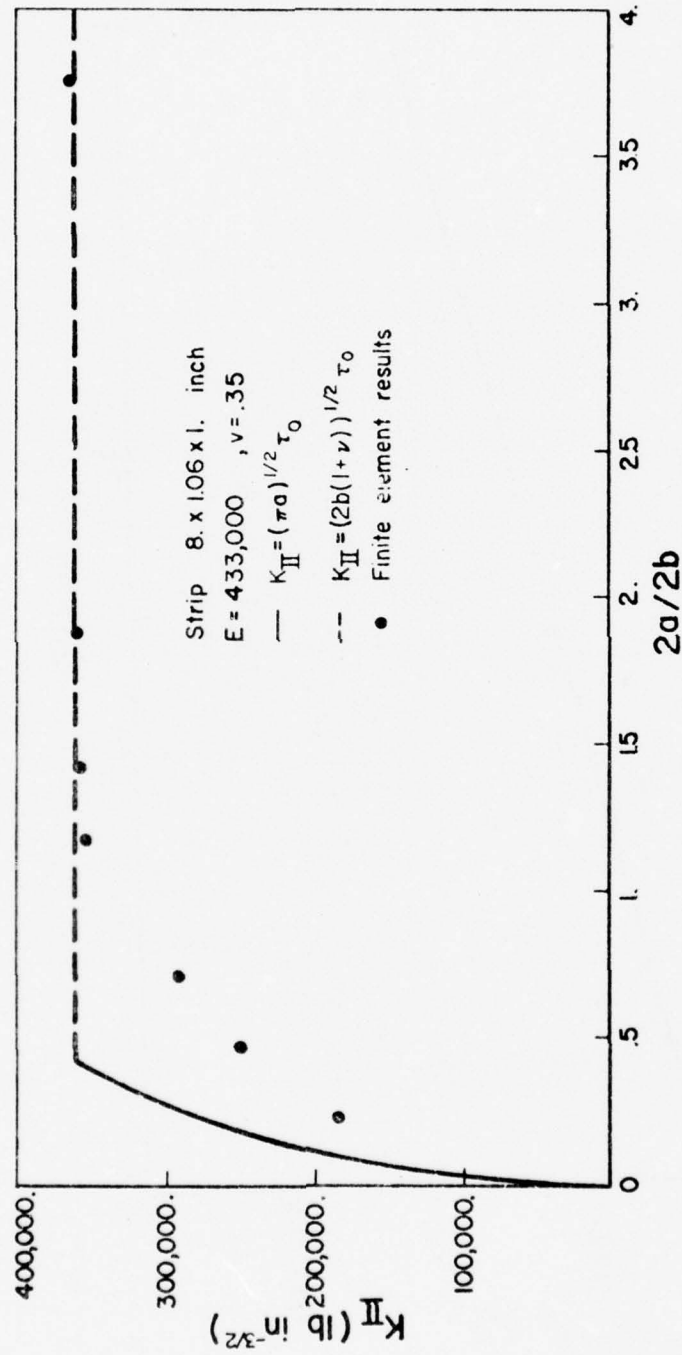
Figure 14. Sliding mode stress intensity factor vs crack length/
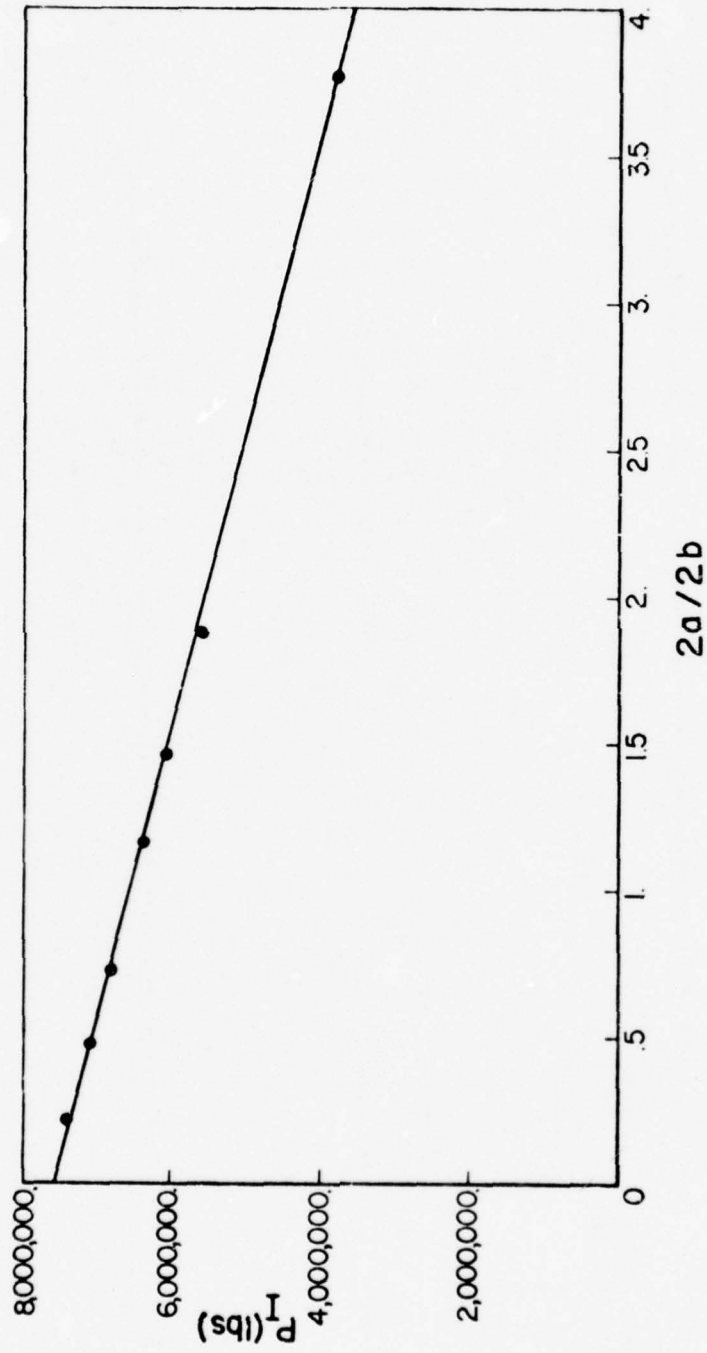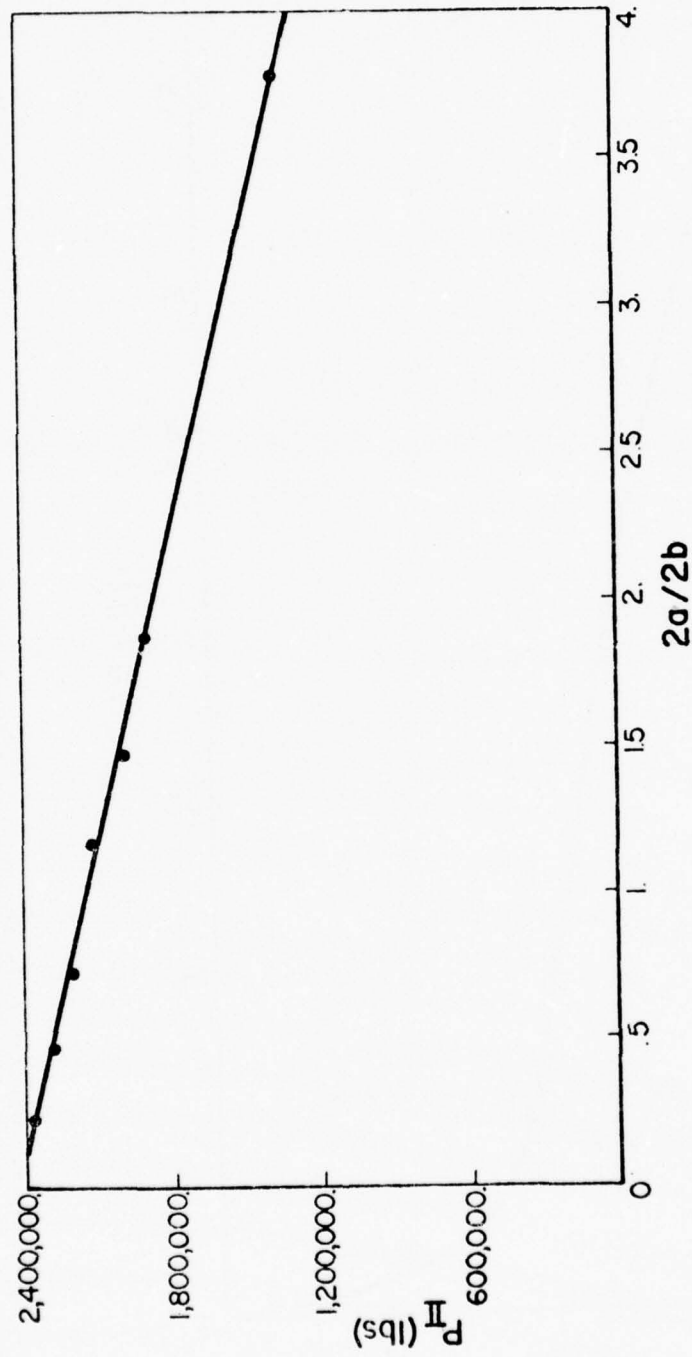strip height for unit displacement.

50

Figure 15. Tension load vs crack length/strip height for unit displacement.

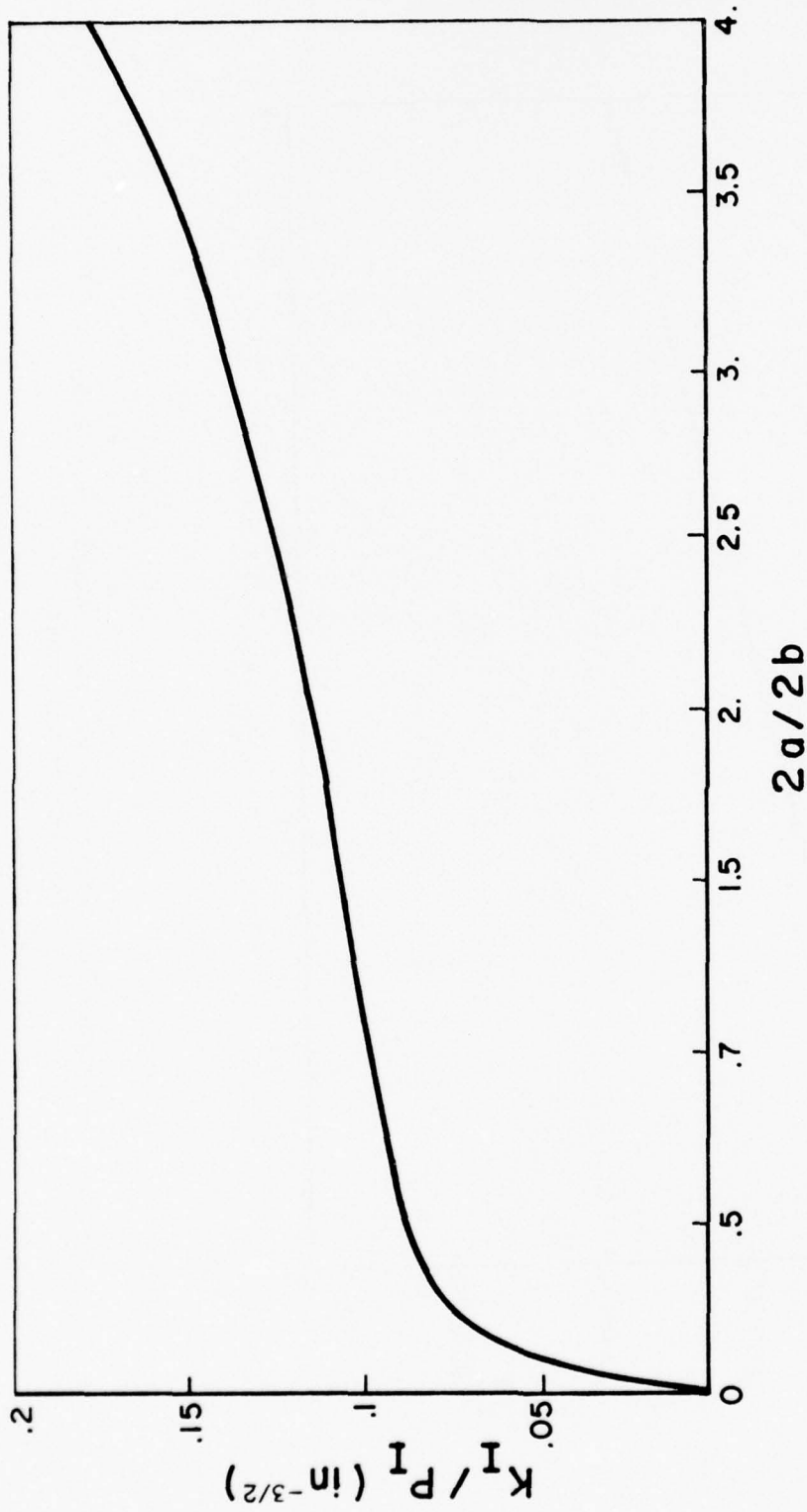Figure 16. Shear load vs crack length/strip height for unit displacement.

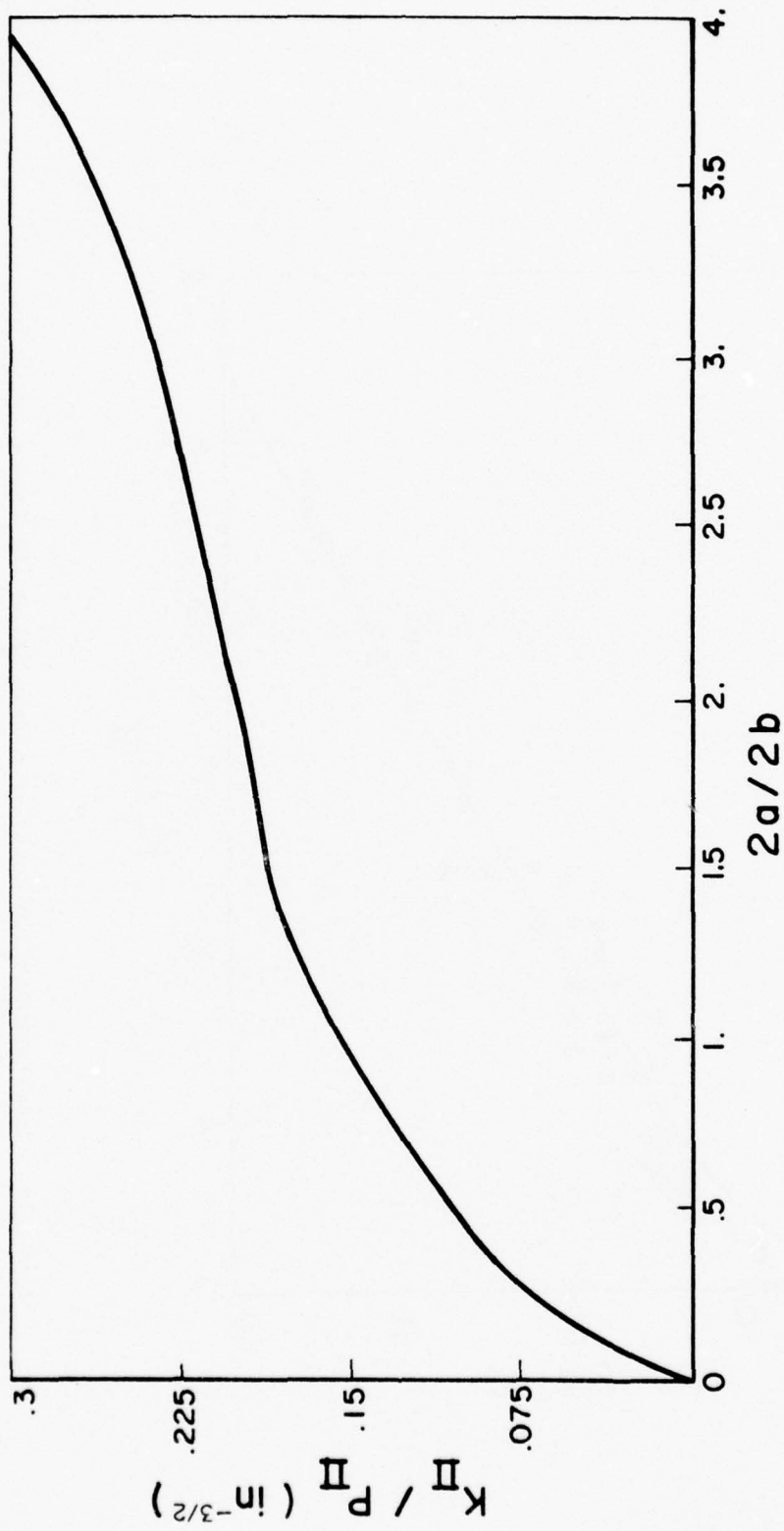Figure 17. Opening mode stress intensity factor/load vs crack length/strip height.

Figure 18. Sliding mode stress intensity factor/load vs crack length/strip height.
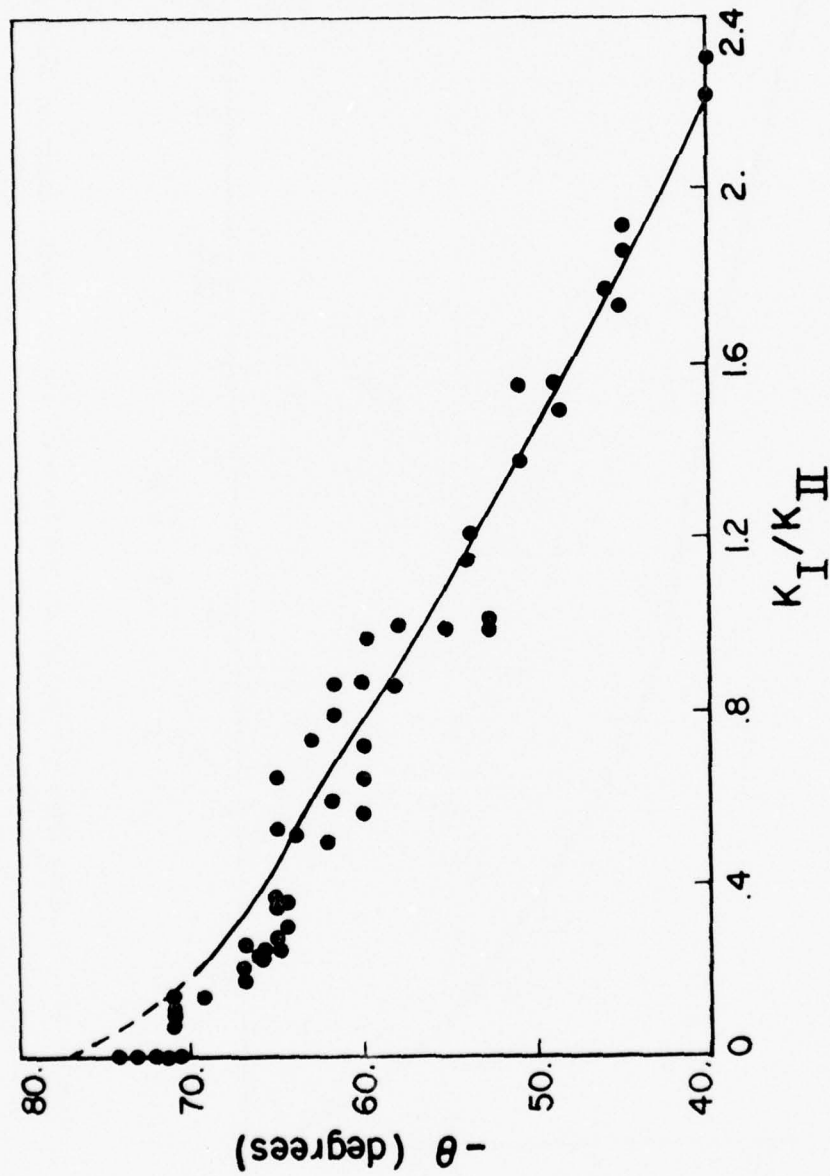
54

Figure 19. Crack propagation angle vs stress intensity factor ratio for theoretical maximum energy release rate [92] and experimental data points.

crack propagation angle. These points were compared to the various theories. The theoretical energy release rate results of Knauss and Palaniswamy [92] compared quite well in certain portions of the data and proved to be best overall. (Referring to Figure 3, it is found that the maximum stress criterion based on the singular solution predicts values which fall along the lower edge of the scatter band in Figure 19.) The dashed line shows the area left incomplete by the theoretical analysis, except for the pure mode II problem.

A plot of the relationship between the stress intensity factors is shown in Figure 20. These points show the problem inherent in most fracture data; viz., a fair amount of scatter. The curve was generated from predictions made by the energy release rate criterion. The criterion fits the data reasonably well and the plot serves as a failure curve for plane problems. However, the maximum stress criterion is slightly better at small angles (cf. Figure 6).

Referring to Figure 19, it is seen that the angle of propagation should be predicted in problems with low K_I/K_{II} in order to complete the solid curve; this will be investigated by the use of energy release techniques with finite element codes in a later section. The reason why a greater load is needed to cause propagation down the interface will also be examined. Also, the ability to predict the angle change as the crack approaches the interface will be studied.
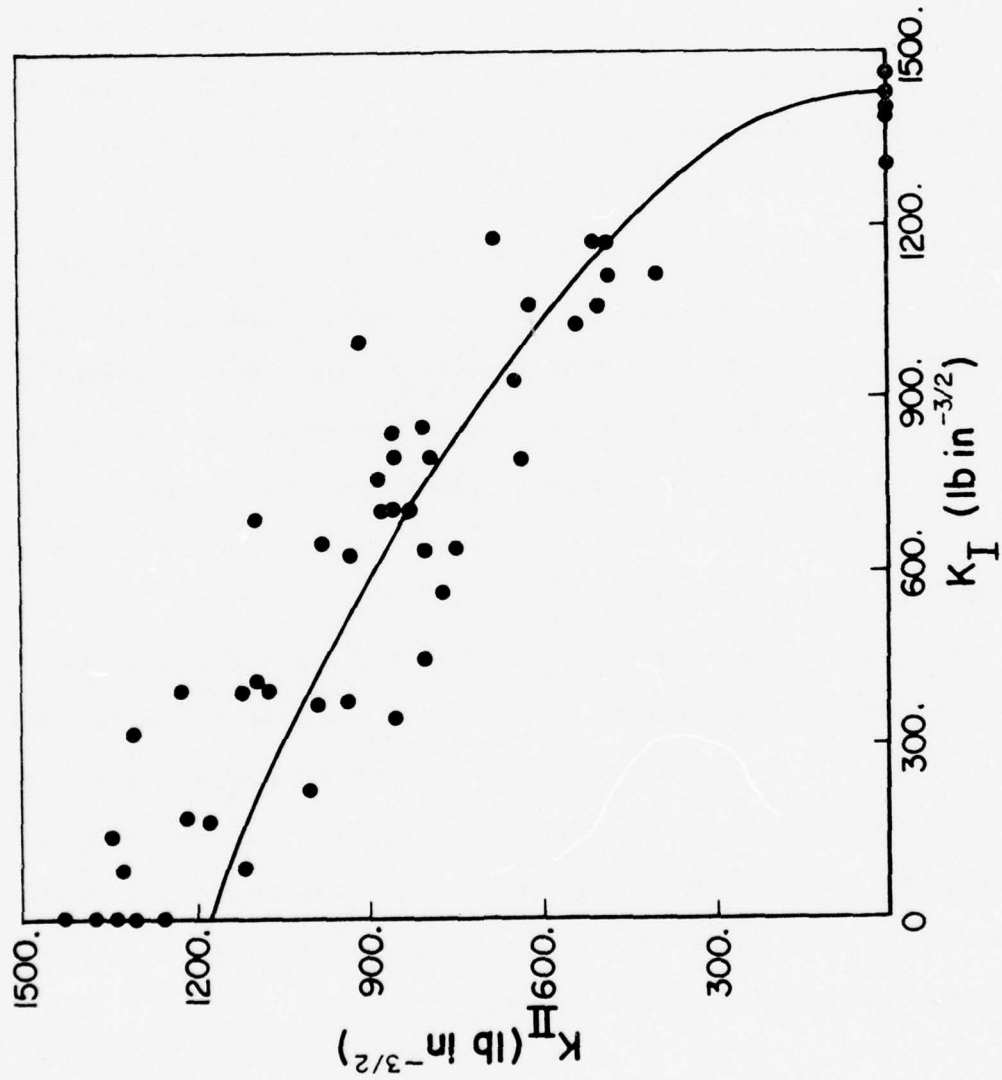
Figure 20. Sliding vs opening stress intensity factors for theoretical maximum energy release rate [92] and experimental data points.

FRACTOGRAPHY

Various interesting observations can be made concerning the crack's path. The tests with the center cracks in either tension or shear without tension provided little new information. The cracks either propagated fairly straight down the center or straight to the boundary. The off-center cracks in tension and shear acted similarly. The off-center cracks in tension propagated along a slight curve to the center of the strip and then down the middle to the ends of the strip as predicted by Erdogan [18]. As described earlier, the center cracks under combined tension (K_I) and shear (K_{II}) propagated on a straight line at a well-defined angle until approaching the interface. Depending on the percentage of tension, the crack would curve to meet the interface. Pictures taken with a bellows-camera system shows this phenomenon in Figure 21.

Using an optical microscope, a Leitz instrument with magnification up to 220X, the angle of propagation next to the intitial tip was examined. The surfaces of the cracks were also examined. The shallow depth of field of this equipment made examination difficult.

A more sophisticated instrument, the JEOL JSM-U3 scanning electron microscope (SEM) was also used. This SEM has a 100 $\overset{o}{A}$ resolution with magnification from 22X to 100,000X. Observations could be made of the samples' surfaces and recorded by the use of photography. The SEM was operated in the secondary electron image mode, with various control settings and magnifications. This mode, where the electrons detected are emitted from the sample or its conductive gold-palladium coating, possesses a great ability for detection of details with a great depth

of field [124]. This instrument was used to investigate the cracks'
angles and surfaces as had others in investigating composite's surfaces
[125,126].

In examining the initial angle up to magnifications up to 10,000X
it was found that there was a very small region where the crack tip
was not perpendicular to the surface of the strip. This was roughly
proportional to the amount of curvature in the initial crack front,
prior to loading. If the initial crack front was curved, the propa-
gating front grew so as to align itself perpendicular to the sheet
surface; the more initial curvature, the greater the distance for
alignment. This region of alignment was very small, usually less
than the sheet thickness. This is shown in Figure 22. The angle of
propagation used was the angle between the initial crack and the crack
path after alignment. After examining a number of crack tips, no correla-
tion could be made between the very small curvature at the initial
crack tip shown in Figure 22 and the craze zone size reported for
plexiglas [121]. No evidence of ductility or crazing marring the crack
surface could be detected.

Investigating the crack surfaces revealed the same appearance
reported as others [127,128]. At slow crack speeds, a large number
of parabolic curves roughen the surface, as speed increases the surface
is smooth, and at speeds approaching the limiting elastic wave velocity
only lines parallel to crack direction can be seen. At the initial
crack tip after the crack front is aligned the surfaces showed the
slow crack velocity markings. The markings then decreased until only
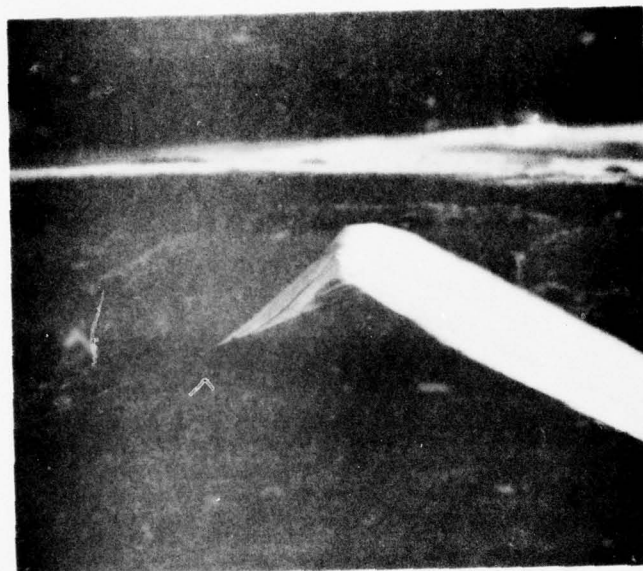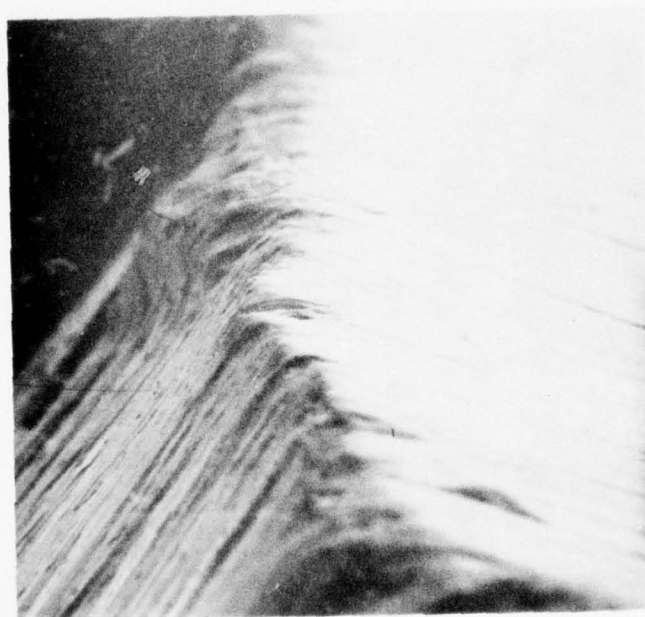the grooves remained, showing increased speed as the crack propagated
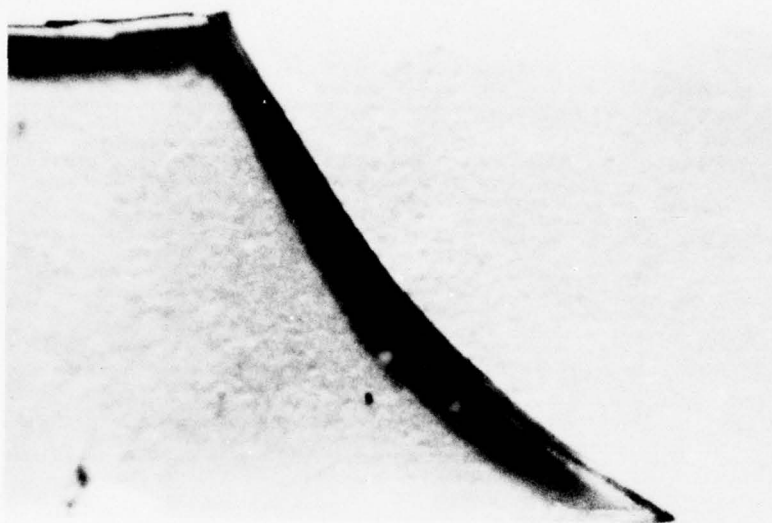
(a)
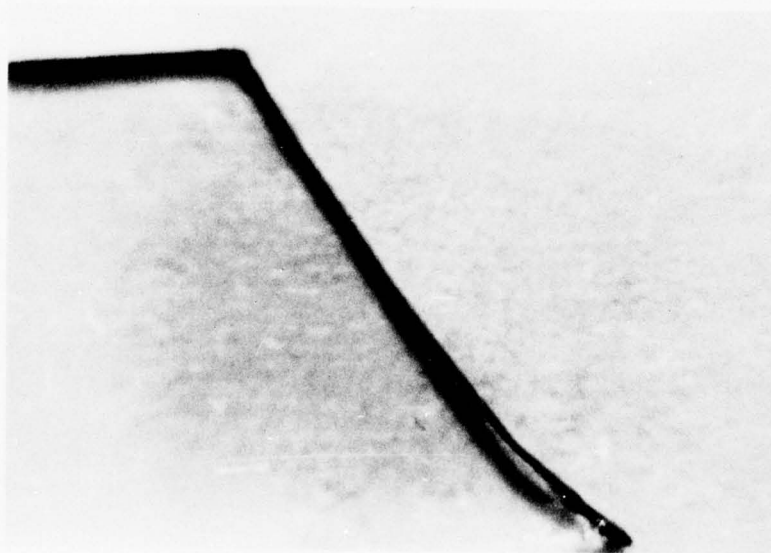
(b)

Figure 21. Photographs (6X) of cracked samples showing crack path
with (a) large K_I/K_{II} and (b) low K_I/K_{II} at failure
(top left is initial crack surface).

(a)

(b)

Figure 22. Micrographs of initial crack tip where (a) shows
alignment distance (100X) and (b) shows initial
crack tip (1000X). The initial crack is the surface
to the right of the crack tip.

61

to the interface. This can be seen in Figure 23. Near the point
where the crack trajectory curved, the markings again appeared indicat-
ing a slowing process. More and more markings appeared, indicating
crack arrest as the crack approached an interface, as shown in Figure
24.

This examination of the crack's surface showed that a properly
made crack is essential in fracture tests. Investigation of surface
features also provided evidence of crack arrest as the crack tip
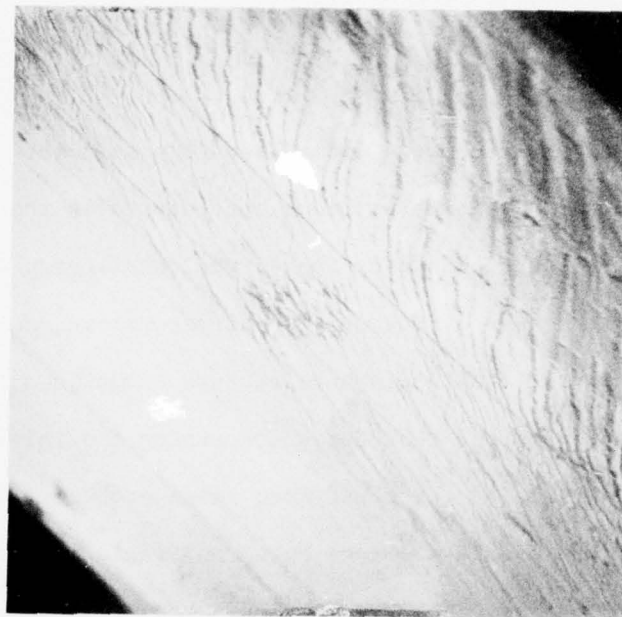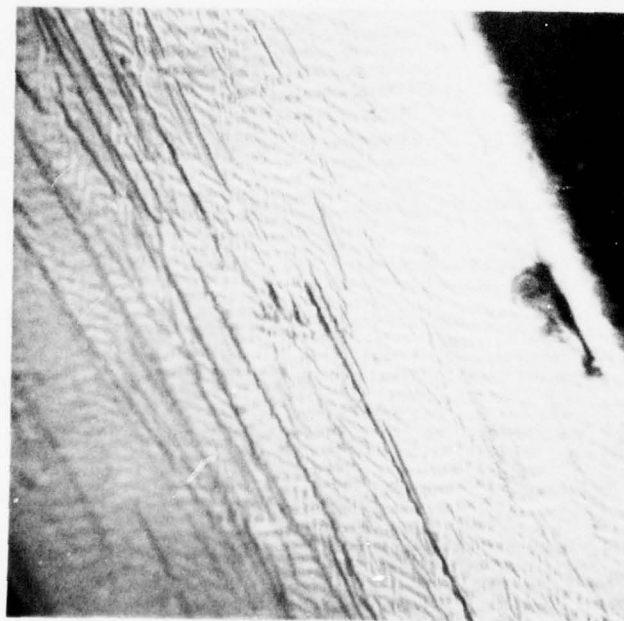approached a bonded edge.

(a)
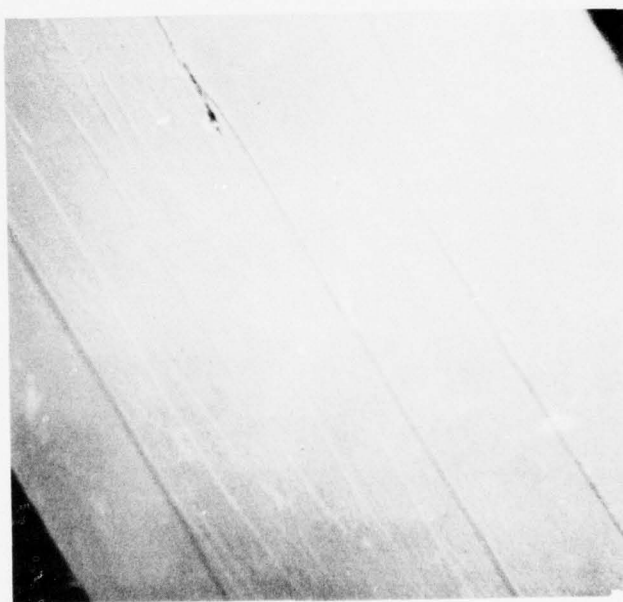
(b)

Figure 23. Micrographs of fractured surfaces showing slow (a)
and fast (b) crack velocity (1000X).

(a)

(b)

Figure 24. Micrographs of fractured surfaces showing fast (a)
and slow (b) crack velocity (1000X).

FINITE ELEMENT ANALYSIS

General

Certain numerical analyses were undertaken to supplement existing
analytical results and investigate problems encountered in the experi-
mental effort. Due to its flexibility in solving complicated problems,
the finite element method was employed. Two different programs were
used. After reviewing the finite element-fracture techniques and using
some of them, it was determined that codes containing special crack
elements would be the best for the mixed mode plane problem. It was
further decided that the hybrid elements based on Pian's work [62]
would be the best for our purposes due to the reasons described in a
previous section.

The first program used was a modified version of the code listed
in Desai and Abel's book [129]. This is a plane strain/stress computer
code which is limited to linear, elastic isotropic bodies. The elements
used are quadrilaterals composed of four linear displacement triangles
(with condensation of the internal node) and linear displacement
triangles. Modifications were two-fold. First, the capacity of the
program was extended by the use of larger arrays and more scratch
files, to allow larger problems to be solved with more elements.
Secondly, the fracture analysis capability was enhanced by calculating
and printing the strain energies of the elements and body, and by
the addition of a crack element to the element library. This ele-
ment is the hybrid crack element presented in the literature [62-
64, 130]. It is compatible with the other elements of the code.
Extensive check problems were investigated to learn the capabilities

and limits to this modified program called CRACK.

In order to solve larger problems more accurately, the Texas Grain Analysis Program, TEXGAP [131], was used, which is a finite element program used for analyzing solid rocket propellant. The version of the code employed here is for linearly elastic plane or axisymmetric bodies. The elements used were reformulated isotropic quadrilaterals composed of four quadratic displacement, linear H triangles (allowing Poisson's ratio to be 0.5 for plane problems), non-reformulated quadratic displacement subparametric quadrilaterals, reformulated isotropic quadratic displacement, linear H triangles, and hybrid crack elements.

In support of the experimental effort, TEXGAP was used to analyze the affect of the bonding geometry on the biaxial stress field. CRACK was used for the determination of the stress intensity factors with some checks made with TEXGAP. Both programs were well-suited for the analysis of fractured bodies.

Biaxial Strip Analysis

A study was made to determine if the experimental crack growth behavior could be predicted. This behavior was divided into three phases. The original configuration of a centered crack was used to determine the initial crack propagation angle. This analysis was then used to predict the change in the angle of propagation as the crack grew. The next phase was to investigate why, after the crack arrested at the interface, increased applied displacement was necessary to cause further propagation along the interface. These three phases were analyzed with the use of the finite element codes mentioned previously.

Due to the limitations pointed out earlier in the crack propagation theories, an examination of the maximum energy release criterion with the use of finite elements was also undertaken. The experimental biaxial strip was modeled with the CRACK program. Two types of analysis were made, one with the use of crack elements and one with only conventional elements.

With the use of two crack elements (one for each crack tip) for a biaxial strip configuration, much experience had been gained in the analyses conducted in support of the experimental work. Additional test problems were conducted to check on the degree of mesh refinement needed to calculate total strain energy. For a uniaxial bar problem, increasing the number of elements from five to forty brought the calculation of strain energy from 99.4% to 99.9% of the exact value of strain energy. Since a comparison of strain energies for a constant mesh was to be made, this error was felt to be negligible. To check the affect of the crack elements on the strain energy, two mesh geometries were used. The refined model used crack elements of one-half the size of the other mesh. Twice as many conventional elements were used about the crack elements in the refined mesh, as compared to the other mesh. Negligible difference was obtained in the angle of the greatest energy release.

Using finite element models of strips of the same proportions as the experimental ones, the strain energies of center cracked and incrementally cracked biaxial strips were analyzed. Varying ratios of applied normal and shearing displacements (corresponding to different ratios of stress intensity factors) along the top and bottom of the two strip

models were applied through a rigid boundary. In the second geometry, the crack increment's length $(0.01 < \Delta A < 0.1)$ and angle were varied to search for the maximum energy release as calculated by:

$$G = \frac{W\ \text{initial} - W\ \text{incremented}}{2\ \Delta a} \tag{16}$$

When G was maximized for a particular angle, this was assumed to be the angle of propagation.

In using this procedure, it was found that only a certain small range of increment lengths would produce a maximum for a particular displacement ratio. The angle of propagation was constant for this range. As the crack propagation angle increased (corresponding to lower K_I/K_{II} ratios) the maximum was harder to determine. It was felt that this was due to the crack element's inability to handle crack tips that were too far from the element's center. Off-setting the element as in Figure 25, helped correct this a little.

Due to these problems, another mesh configuration using only conventional elements was used as in Figure 25. This mesh was used to check and correct some of the previous answers, especially for cases involving low K_I/K_{II} ratios. In this geometry, the crack tip's nodal point was changed for various angles and increment lengths to determine the maximum value of G. This method was less sensitive to changes in increment lengths and allowed a more reliable method of determining the maximum energy release, G, and the angle of propagation, θ.

The question of using a finite increment for calculating G must be faced. Due to the finite element representation, some finite value has to be used. The ratios of maximum G for combined mode to the G
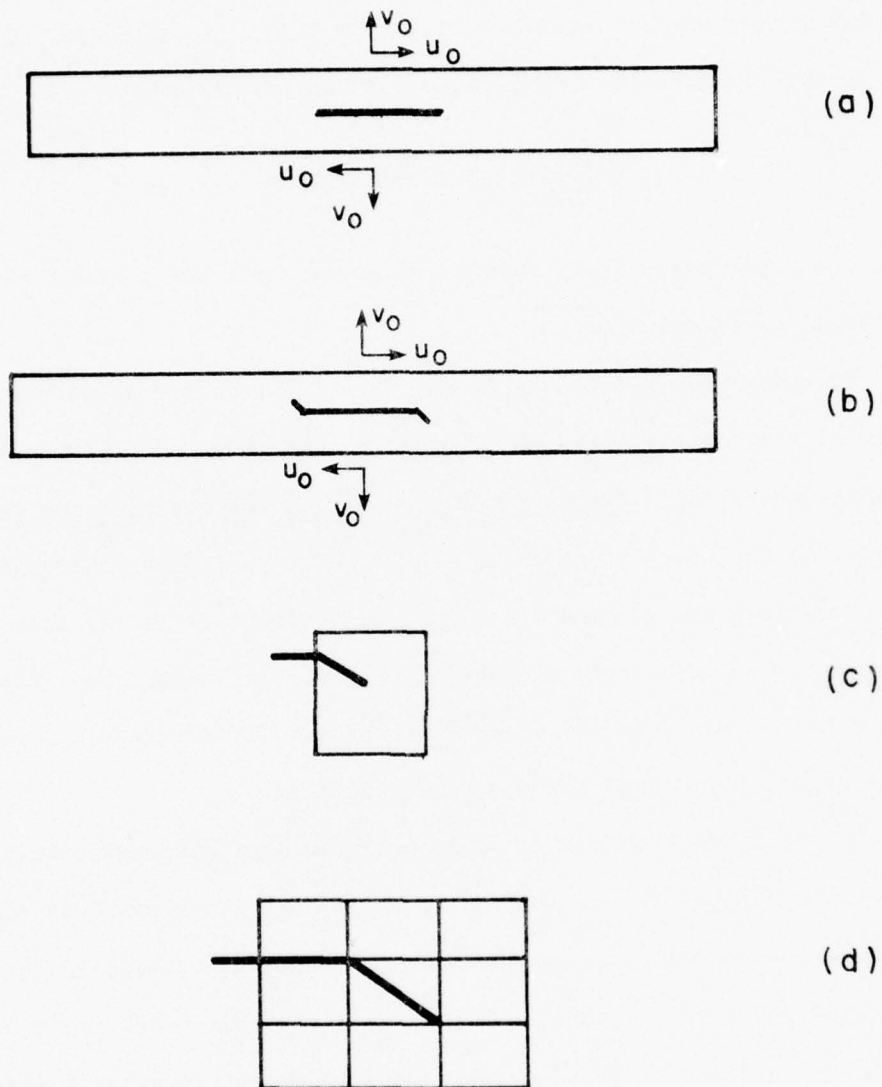
Figure 25. Finite element crack models: initial crack (a), incremented crack (b), off-set crack tip element (c), and crack tip modeled with conventional elements (d).

for opening mode for this analysis were calculated. Comparison to the
values from Hussian's et al. [95] theoretical analysis for a virtual
(approaching zero) increment, the ratios were in close agreement. The
finite element results were therefore below those given in [92] (cf.
Figure 6).

The results of examining this first phase of crack propagation are
presented in Figure 26. The initial angle of propagation is plotted
against the ratio of stress intensity factors for the original crack.
This curve, while calculated from data for a specific geometry,
can be used for any two-dimensional crack problem. It can also be
compared to the experimental results of this report as in Figure 19,
as well as the results of other theories. The results for this finite
element analysis are slightly lower than that of Knauss and Palaniswamy's
analytical results [92], but agree well with Coughlan and Barr's [96]
finite element results. The results also provide θ over the range of
values of K_1/K_2 not fully covered in other researcher's analyses. The high
range of values of K_1/K_2 were not investigated due to the agreement
already found in the literature.

With the first phase of crack propagation completed, the analysis
of the crack that has propagated part-way to the clamped boundary was
made. Two cases were examined, based on the initial angle of propa-
gation. These angles were 75° and 55° corresponding to initial stress
intensity factor ratios, K_I/K_{II}, of 0. and 1.1. The program TEXGAP
was used in this analysis. The crack geometry used for the finite
length angled crack tip is shown in Figure 27. The other crack tip
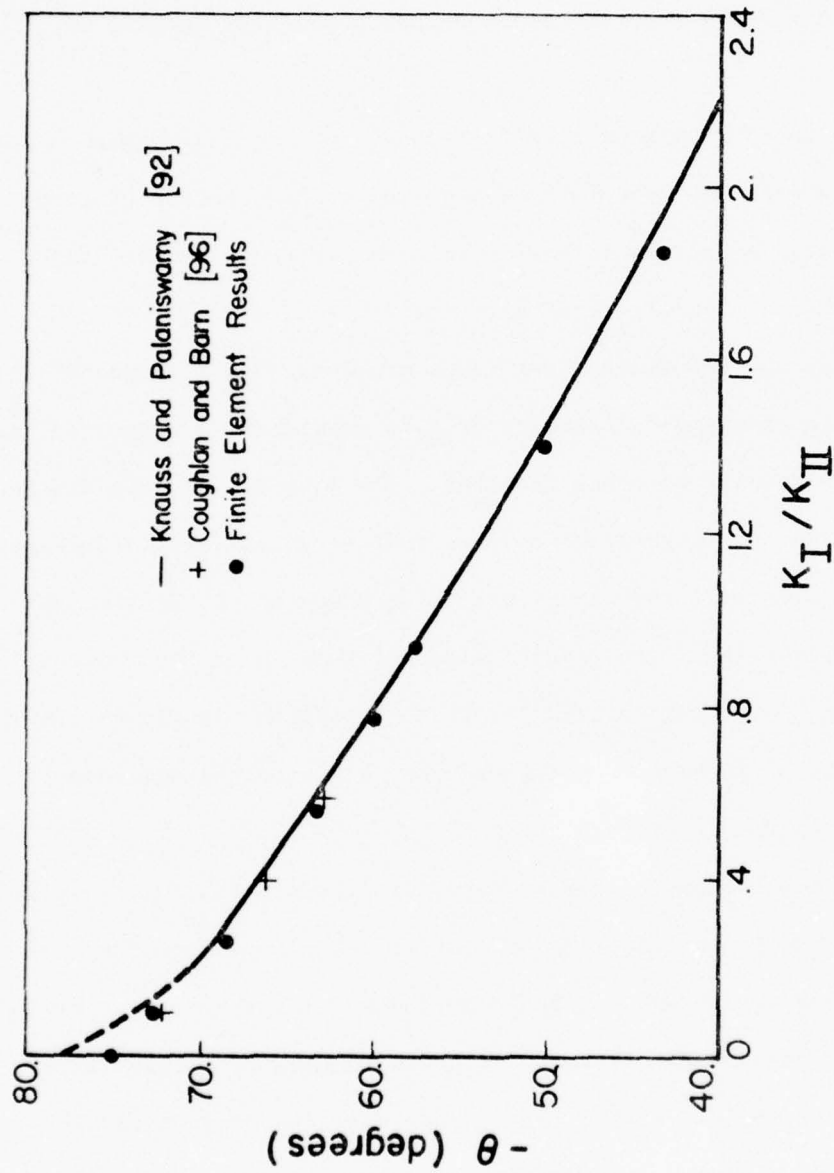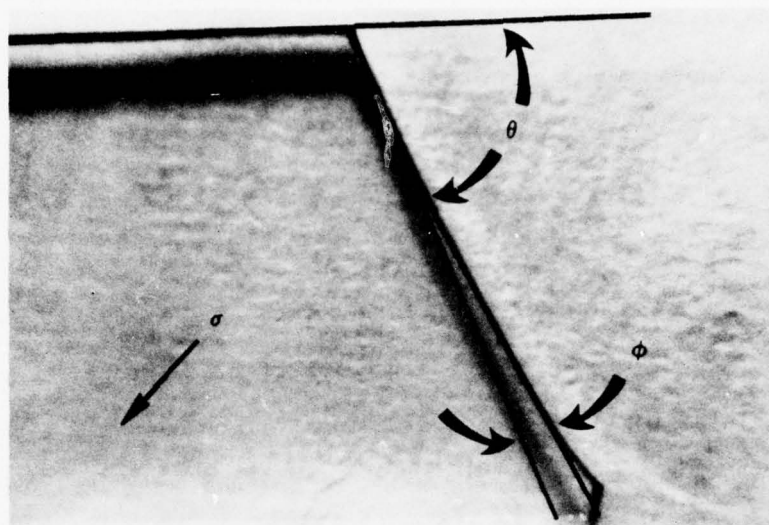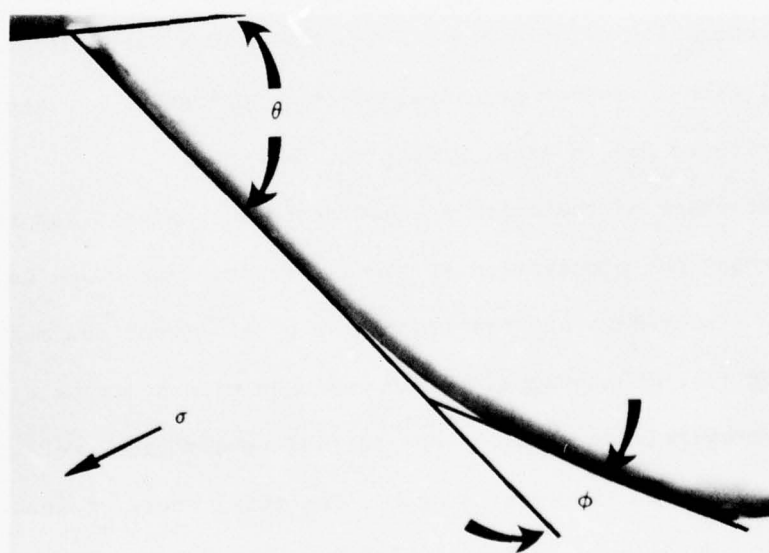was also incremented but not modeled with a crack element. The crack

Figure 26. Crack propagation angle vs stress intensity factor ratio for finite element results compared against other criteria.

Figure 27. Finite length angled crack and angles of propagation for shearing (a) and combined mode (b) problems.

element size was varied as also the number of elements behind and ahead of the crack element were increased. Little change in answers were found. The displacements required to produce the initial stress intensity factors were also applied to the biaxial strip with the angle crack. The new stress intensity factors for this geometry were then obtained.

These new stress intensity factors formed a K_I/K_{II} ratio which could then be used to predict the direction of crack propagation. The predicted initial angle of propagation ($\theta=55°$) produced a new ratio of 2.9 with a new propagation angle, $\phi=32°$, to the angled crack line of propagation; the angles shown in Figure 27b are 52° and 24°, respectively. The mode II problem ($\theta=75°$) had a new ratio of 18.5 with a new propagation angle of $\phi=5°$; from Figure 27a, these angles are 70° and 6°, respectively. These new propagation paths did not align themselves perpendicular to the direction of global maximum principal stress, indicating the need of a local criterion to govern crack direction.

The next phase of the crack's behavior to be analyzed was the matter of arrest and propagation at the interface. Two cases were considered: cracks with propagation angles of 65° (combined mode) and 75° (mode II). The program TEXGAP was used with no crack elements. The total energy release rates at the initial center crack were calculated for a certain increment length. The total energy release rates were in approximate agreement with Hussain's et al. [95] energy release rate mentioned earlier. The crack was then allowed to propagate to the interface by means of disconnecting elements. The

energy of this configuration was determined for the same applied displacements as the initial crack. The energy release rate along the interfaces was then calculated for the same increment length as for the initial crack to avoid any effect of numerical errors.

For specified applied displacements, the total energy release for the center crack was 2.1 times the energy release for propagation along the interface for the combined mode case. The sliding mode case had a ratio of 3.4. Assuming the initial crack and interface crack propagates at the same critical value of the total energy release rate, the crack arrests at the interface.

In order to calculate the displacement required to propagate a crack along the interface, it is helpful to draw upon the linearity of the problem. Namely, in view of this linearity, the relation between the total energy release rate and the applied displacements can be written:

$$G = \gamma_{11} u_o^2 + \gamma_{12} u_o v_o + \gamma_{22} v_o^2 \tag{17}$$

where γ_{11}, γ_{12}, and γ_{22} are independent of u_o and v_o. In the case of the sliding mode, the ratio of displacement needed to propagate the crack along the interface to that for the center crack is easily found to be $\sqrt{3.4} = 1.84$ since $v_o = 0$ in this case. Table 2 shows the comparison of the analytical and experimental values of increased displacement needed to cause further propagation.

Table 2. Percent of Initial Displacement Needed to Cause Interface
Crack Propagation.

	Analytical	Experimental
Mixed Mode	188%	175-200%
Shearing Mode	184%	175-200%

The range of values for the experimental results is due to the varia-
bility of the cohesive bond between the plexiglas plates and sheets
as described in the experimental section of this study.

From the previous discussion, it is believed that the crack path
can be predicted in the biaxial strip model of a composite. For this
model with very stiff or rigid fibers, it has been demonstrated that
cracks will propagate toward the boundary provided some of the growth
is of the second mode (sliding mode). It also has been shown that this
propagation path can be predicted. The crack arrests at the boundary
and increases in applied displacements must be made to cause further
crack growth. With a crack arrest mechanism described for composites
with combined mode and shearing mode microcrack propagation, a crack
arrest mechanism for opening mode microcrack propagation must be
explored. This will be done by considering fiber flexibility.

Simulated Composite Analysis

A natural extension of the previous analysis is to go to a model
with flexible fibers. The motivation for this is to calculate the
energy release rate due to fiber bending and to show the affect on
crack growth, especially on cracks in an opening mode situation. In

this simple model of a composite subject to loads at infinity, the fibers just above and below the crack tend to respond as beams on an elastic foundation. With no crack present, the fibers would just separate slightly. With a crack, the crack is equivalent to an internal pressure (equal and opposite to the stress in an uncracked body) acting between the fibers of an externally unloaded specimen, thus causing local bending.

This approach was taken in a previous analysis using a simple model of a beam on an elastic foundation [8]. For the case of a uniformly loaded fixed-ended beam on an elastic foundation [132], the deflection and loading was used to calculate the strain energy release rate due to beam bending. The relationships between energy release due to beam bending, crack length, and fiber rigidity were explored.

A simple but more realistic model of a composite exhibiting fiber bending was needed. A finite element representation of the geometry in Figure 28 was examined using TEXGAP. The cases were examined either as pure opening mode or as pure sliding mode where uniform displacements were applied at the fixed boundary. Only the right half of the problem was modeled with the use of the crack element, taking advantage of the symmetry of the problem. Test cases of different dimensions were run to ensure the model was long enough to be infinitely long. In this case, a size of 5. x 40. was needed for the total model.

The problem was analyzed as if it were in plane stress; for plane strain (plates in bending) the results would be qualitatively the same and plane strain results can be extracted from the plane stress analysis by an appropriate change in the material constants. The material constants used in this analysis are those typical of a graphite
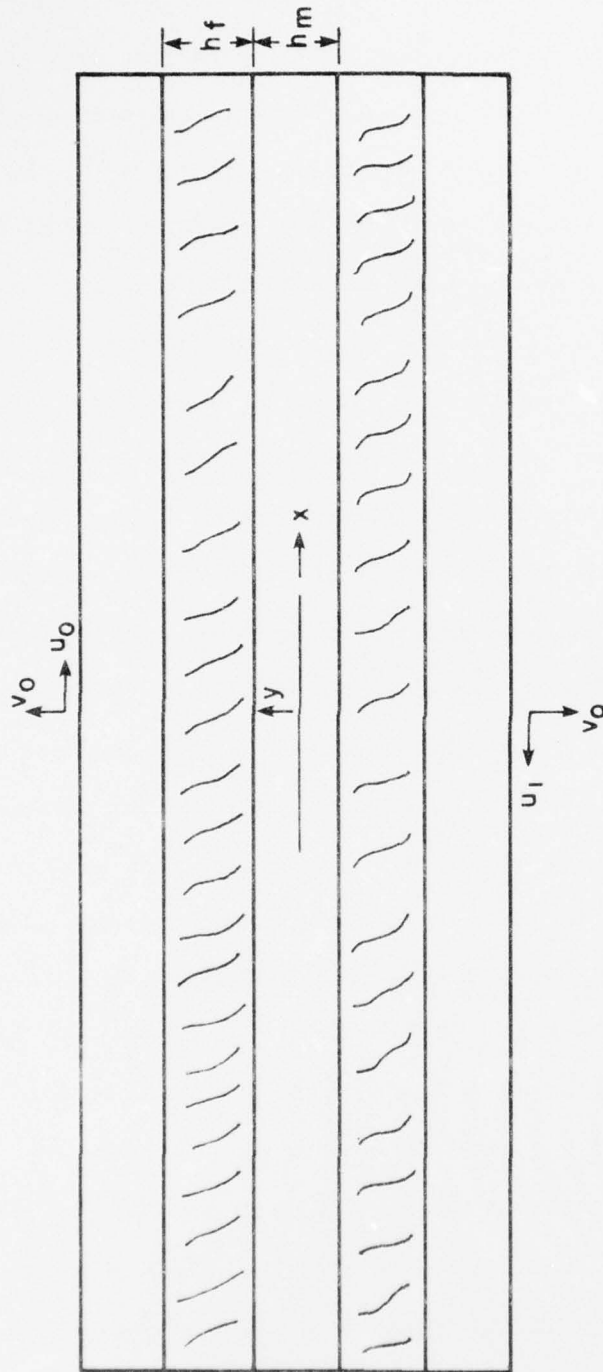
Figure 28. Flexible fiber model with crack of length 2a and fiber properties (E_f = 40. x 10^6, ν = .2, h_f = 1.) and matrix properties (E_m = 5. x 10^5, ν = .35, h_m = 1.). Actual size of model is 5. x 40.

fiber-reinforced epoxy matrix. For equal fiber, h_f, and matrix, h_m, heights in an idealized circular fiber composite [8], the fiber volume fraction, V_f, is computed by

$$\frac{h_f}{h_m} = \frac{\sqrt{V_f}}{1-\sqrt{V_f}} \tag{18}$$

which gives a value of 0.71, not unreasonable for advanced composites.

The deflection in the fiber's y-direction about the crack tip for a uniform vertical grip displacement v_o are presented in Figure 29. As can be expected, no fiber bending occurred in the shear case and it will not be presented. For small cracks, the center line deflections of the fiber are not large, but their bending extends almost ten times the crack length. With increases in the initial crack length, or as the crack grows, the deflection gets much larger, but the length of the fiber affected only slowly increases. As the crack approaches a length of ten times the fiber height, the portion of the fiber above the crack deflects nearly as much as the applied displacement. (This is due to the use of a uniform grip displacement.) The effect along the fiber is only over twice the crack length. As the crack gets larger, the deflection does not get larger, but the length of the fiber affected beings to slowly increase.

Values of the total energy release rate G_T, were calculated from the stress intensity factors (from the finite element analysis) by

$$G_{TI} = \frac{K_I^2}{E_m} \quad \text{or} \quad G_{TII} = \frac{K_{II}^2}{E_m} \tag{19}$$
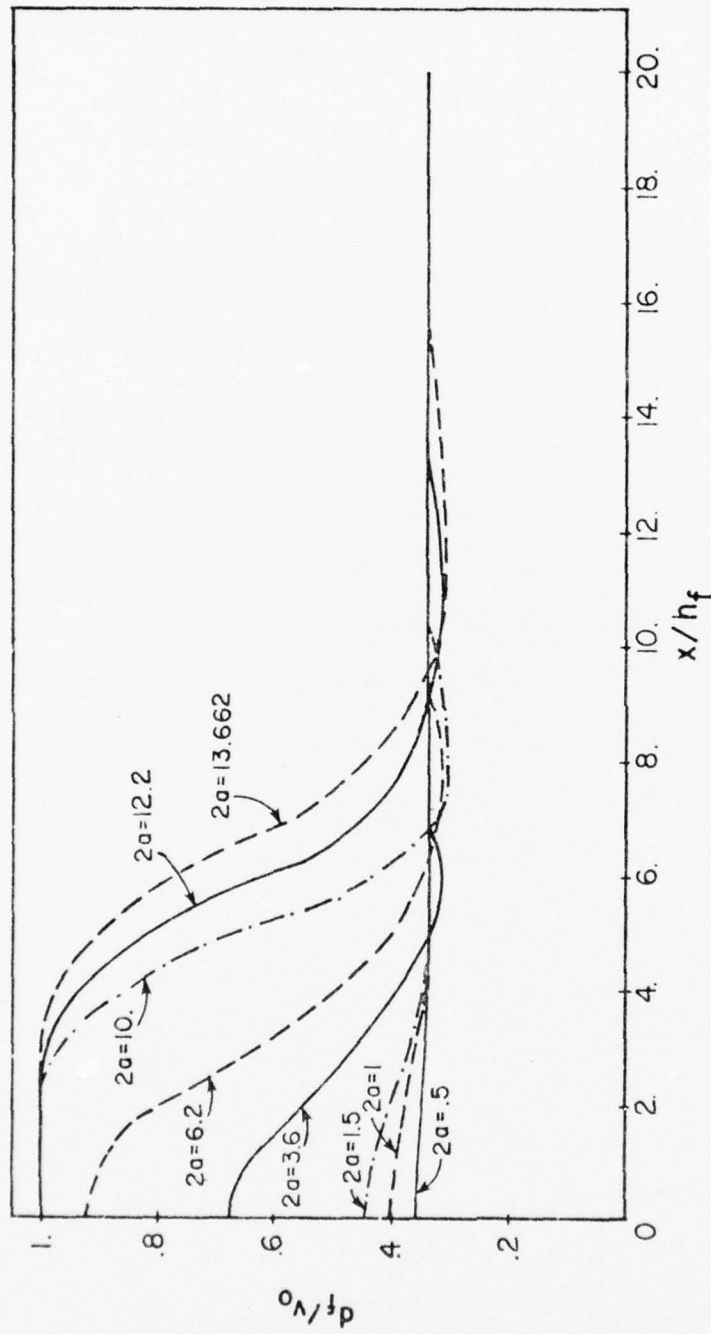
Figure 29. Mid-fiber deflection/applied displacement vs distance along the fiber/fiber height for various crack lengths.

where E_m is the matrix modulus; it is to be noted that since the virtual increment of crack growth lies within the matrix material, only the matrix modulus appears. The energy release rate due to fiber bending, G_B, can then be defined as the difference between the total energy release rate and that due to matrix stretching G_I, or shearing, G_{II}, with rigid fibers; viz

$$G_{BI} = G_{TI} - G_I$$

or (20)

$$G_{BII} = G_{TII} - G_{II}$$

The total energy release rate's are plotted in Figures 30 and 31. The two energy release rates (opening and sliding) are normalized with respect to the strain energy release rates for the rigid fiber case as [8]

$$G_I = \frac{h_m \sigma_o^2}{2 E_m} (1 - \nu_m^2)$$

(21)

$$G_{II} = \frac{h_m \tau_o^2}{E_m} (1 + \nu_m)$$

These normalized values are plotted against a dimensionless quantity derived in [8] reflecting the fiber rigidity and crack length:

$$\gamma = a \left(\frac{4k}{E_f I}\right)^{1/4}$$

(22)

$$I = h_f^4 / 12$$
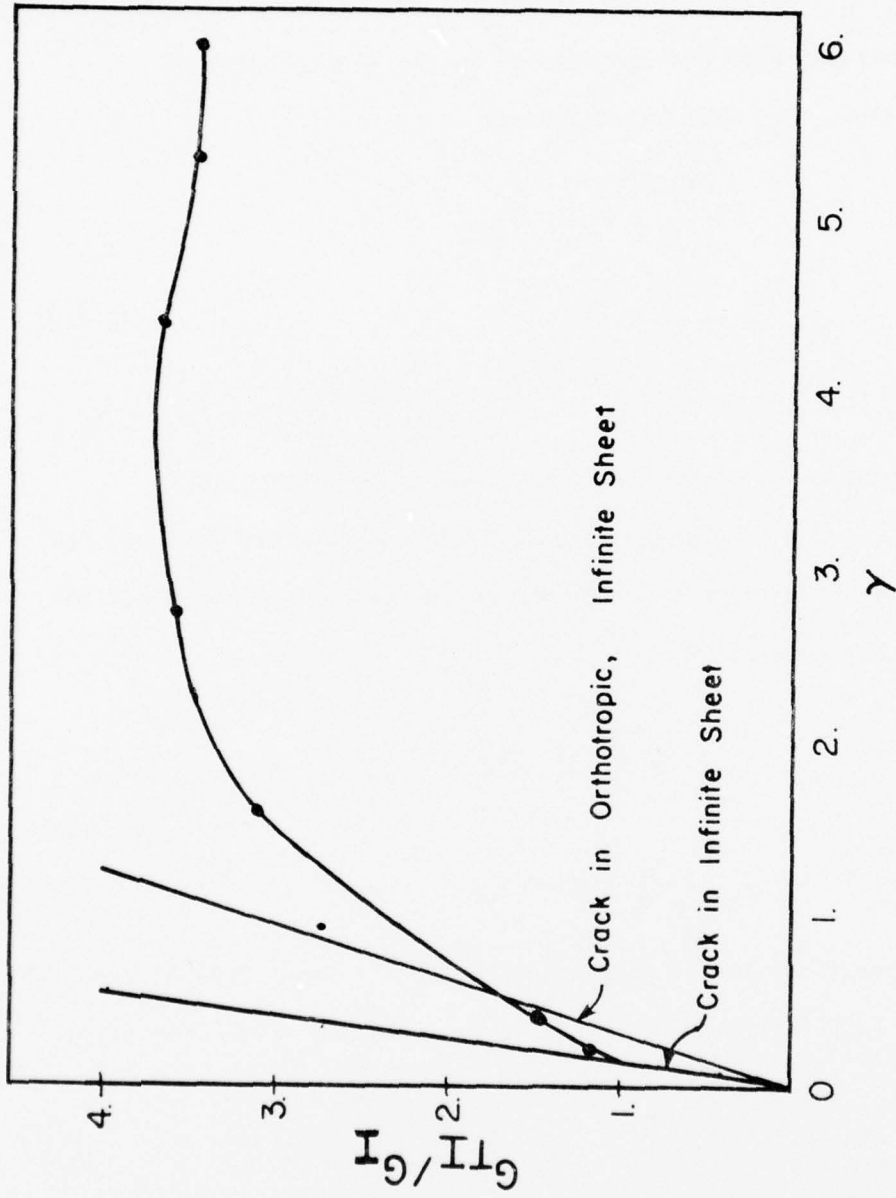
Figure 30. Energy release rates vs γ for opening mode. (——finite element solution)
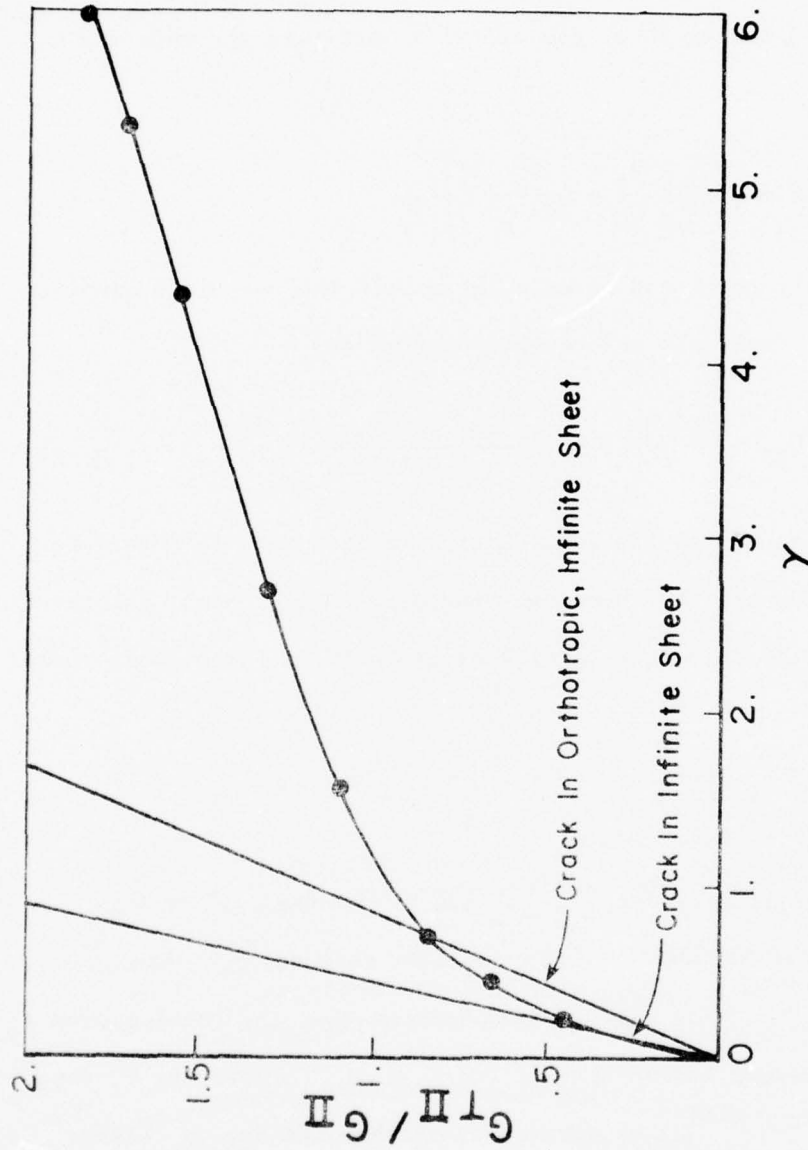
Figure 31. Energy release rates vs γ for sliding mode. (•——• finite element solution)

where k is the foundation stiffness and I is the fiber's area moment of inertia. The value of k for this analysis and for an actual composite could be treated as a free parameter used to correlate theory and experiment. For the circular-fiber composite, an estimate was made for k in [8],

$$k = \frac{E_m}{(1+\nu_m)} \frac{h_f}{h_m} = \frac{E_m}{(1+\nu_m)} \frac{\sqrt{V_f}}{1-\sqrt{V_f}} \tag{23}$$

A better estimate for k can be calculated with the use of an equation derived in the previously referenced research [8],[*]

$$G_{BI} = \frac{\sigma_o^2 h_f}{k} \left[\frac{2(\cosh^2\gamma - \cos^2\gamma)}{(\sinh\gamma + \sin\gamma)^2} - 1\right] \tag{24}$$

Figure 30 shows how the total energy release rate in Mode I is strongly affected by fiber bending. For very small cracks, the results are bounded by the release rate of a crack in an infinite sheet given by

$$G_{I\infty} = \frac{\pi a \, \sigma_o^2}{E_m} \tag{25}$$

As the crack length increases, total energy release rate follows the same qualitative shape as for the energy release rate due to fiber bending calculated in [8]. For sufficiently long cracks, the total energy release rate becomes independent of crack length as does the bending energy release rate. The magnitudes of the bending energy release rates at these crack lengths could be predicted by the equations

*The factor of 2 in the brackets was inadvertently omitted in the final typing of [8].

derived in [8] with a reasonable value of k (490,000 psi, which is coincidentally close to the value of the matrix modulus).

Figure 31 shows how the total energy release rate in the Mode II problem increases without bound; there is little effect of fiber bending. It too is bounded for very small cracks by the energy release rate for a crack in an infinite sheet given by

$$G_{II_\infty} = \frac{\pi a\ \tau o^2}{E_m} \tag{26}$$

The energy release rates for an orthotropic body were calculated using the effective properties of the material used in the finite element analysis and are shown in Figures 30 and 31. The details of this analysis can be found in the Appendix. This was undertaken to examine the relationship between the overall composite's and fiber model's energy release rates. The equations for the plane stress energy release rates [133] are

$$G_I = K_I^2\ \left(\frac{a_{11}\ a_{22}}{2}\right)^{1/2}\ \left[\left(\frac{a_{22}}{a_{11}}\right)^{1/2} + \frac{2a_{12} + a_{66}}{2\ a_{11}}\right]^{1/2}$$

$$\tag{27}$$

$$G_{II} = K_{II}^2\ \frac{a_{11}}{(2)^{1/2}}\ \left[\left(\frac{a_{22}}{a_{11}}\right)^{1/2} + \frac{2a_{12} + a_{66}}{2\ a_{11}}\right]^{1/2}$$

where the a_{ij}'s are the material constants for an orthotropic body. Using the stress intensity factors for the crack in an infinite sheet, these release rates predicted much larger values than that of the fiber bending model. This indicates the importance of fiber bending, and that many fibers may be affected by even one crack.

Further Results

Using the results from the rigid fiber models, some observations can be made as to crack growth and arrest. Assuming that the energy per unit area, Γ, required to produce new surfaces, is independent of loading, crack growth will occur when $G_T > 2\Gamma$ and arrest when $G_T < 2\Gamma$. Considering the entire crack front, the point of initiation of crack growth will be where this criterion is met.

In order to determine how fiber bending affects crack extension of an initially centered crack, K_I/K_{II} was plotted vs γ, in Figure 32, for equal far-field tension and shear stresses. The rigid fiber model results are also plotted for comparison. For very small cracks, the crack behaves as if it were in an infinite sheet, with $K_I/K_{II} = 1$, corresponding to a crack propagation angle of approximately 55° (from Figure 26). For somewhat larger initial cracks, their behavior becomes affected by fiber bending, in that $K_I/K_{II}=1.6$, corresponding to a crack angle of approximately 47°. The rigid grip solution with $K_I/K_{II} = 0.57$, indicates a crack propagation angle of approximately 65°. This variation in angle will not unduly affect crack propagation; the crack will still propagate to the fibers at a fairly steep angle and will then arrest at the fibers. These changes in stress intensity factor ratios due to fiber bending will also have an affect on crack initiation. The change in ratio changes the point of failure on the K_I/K_{II} interaction curve as in Figure 6. A higher ratio would involve greater applied stresses to cause crack propagation.

Of great interest is arrest mechanisms for opening mode cracks. One possible mechanism is the propagation of cracks in adjacent matrix
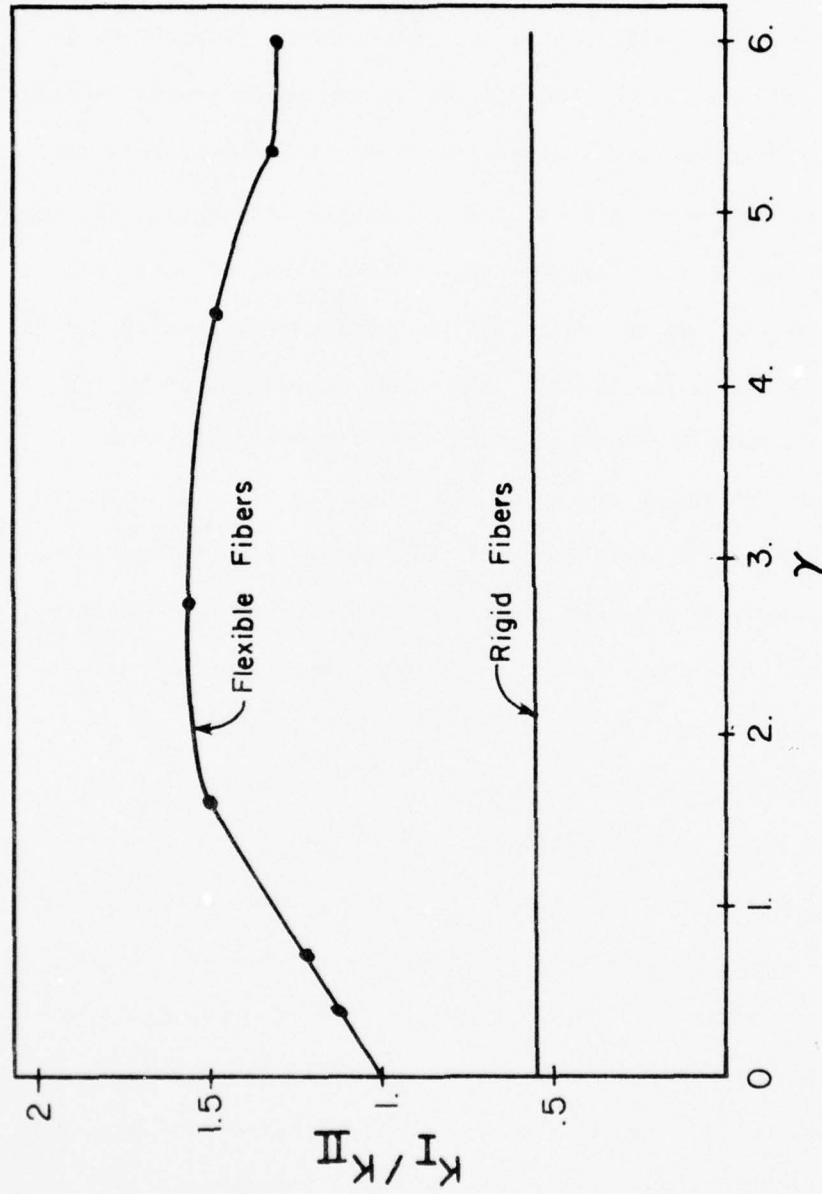
85

Figure 32. K_I/K_{II} vs γ for $\sigma_o = \tau_o$.

areas. The shear stresses produced in this neighboring matrix, caused by fiber bending, helps to cause cracks to grow from pre-existing flaws, cracks of sufficient length to relieve the stresses at the tip of the initial crack. As seen in Figure 33, the shear stress directly above the crack tip increases and then levels off as the crack length increases. The relative magnitude of the shear stress to applied stress is small, but a small amount of increase in a stress concentration can be significant in determining crack initiation; three dimensional effects will probably increase this stress concentration. Related crack skipping has been observed experimentally [8,23]. The shear stress caused by fiber bending within the matrix about the crack is of some significance. The shear stresses above the crack tip and below the fiber are plotted in Figure 33. For an off-centered crack, a shearing mode contribution can be added to what had previously been only opening mode propagation. This will then turn the crack toward the fibers, causing crack arrest.

As the crack continues to grow, either in the interface between the fiber and matrix or in the matrix, the growth will continue to be controlled by the neighboring fibers. Comparison of the energy release rates of the fiber model and those for the homogeneous orthotropic model, in Figures 30 and 31, shows that a cracked composite will require much higher applied stresses for small cracks to propagate than had been predicted by using the latter theory. This indicates that the crack must be very large, compared to the fiber spacing and diameter discussed here, in order to treat the material as homogeneous.

Comparison of energy release rates and stress intensity factors have lead to some conclusions on microcrack growth and arrest in
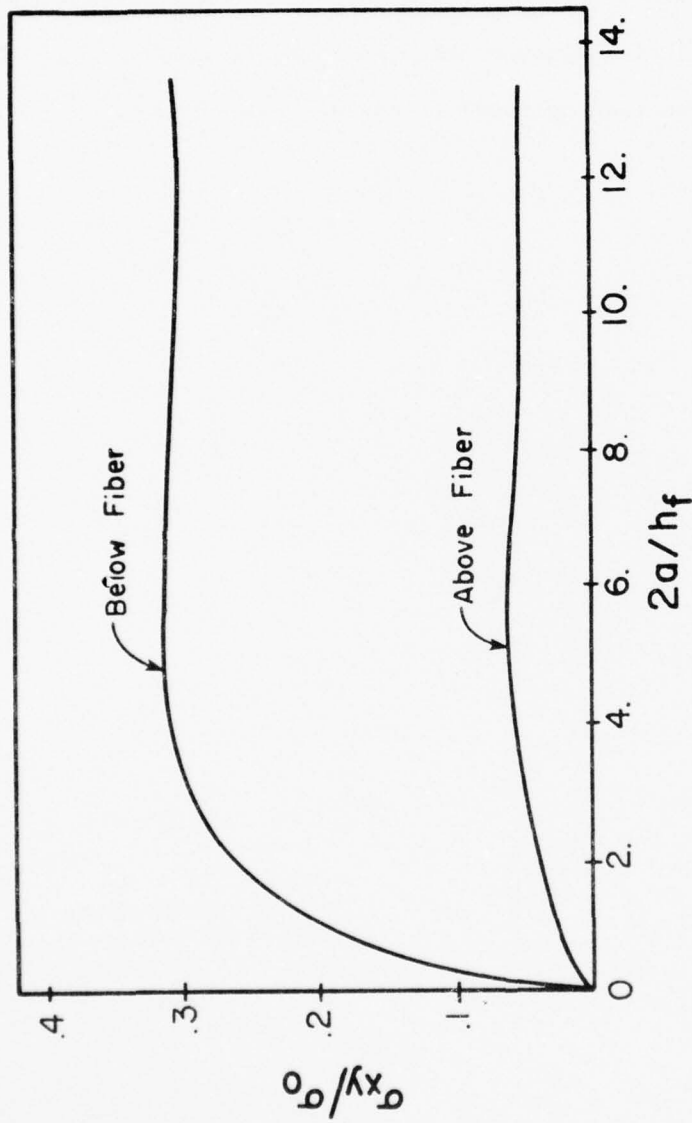
Figure 33. Maximum shear stresses above crack tip just above and below the fiber vs crack length, for opening mode problems.

fibrous composites. The simple models used here have neglected many aspects of real composites such as fiber randomness, flaw size distribution and interface inhomogeneity. The complex, real three-dimensional problem was also approximated with *two-dimensional* models. Even with these approximations, it is believed that these models portray some of the features of microcracking found in the actual composite.

CONCLUSIONS AND RECOMMENDATIONS

After examining the literature, it was concluded that of all existing criteria, the maximum energy release rate criterion had the strongest physical basis and best correlation with data, especially for brittle materials. The usefulness of the finite element method in fracture mechanics analysis has also been demonstrated in the literature surveyed. The maximum energy release rate criterion was extended to those combined mode fracture problems which are largely composed of the shearing mode. This was accomplished with the use of the finite element method and supported with experimental evidence provided with a test geometry not previously used for combined mode problems.

This completed criterion was then used to predict the crack paths and stress intensity factors interaction in long rectangular strips of plexiglas clamped on the long edges. The predictions compared favorably with experimental evidence. By correlating energy release rates of cracks initially in the center of the strip with cracks already propagated to the long edges, it was calculated and experimentally verified that significantly increased displacements were necessary to continue crack growth.

Building upon the biaxial strip model (or rigid fiber model), the affect of fiber flexibility on crack arrest was explored. Fiber bending decreased the tendency of the crack to propagate toward the fibers, but supplementary crack mechanisms resulted. These came about due to the shear stresses induced by bending; shear stresses in adjacent matrix regions possibly causing crack skipping and shear stresses

in the matrix about the crack causing propagation toward the fibers, both resulting in increasing the tendency for crack arrest. Drawing upon both the rigid fiber and flexible fiber models used, the nature of crack growth from a small defect to a crack whose dimensions are comparable with fiber spacing was discussed.

Examination of fractured surfaces, obtained from the experimental tests, showed that the direction of initial crack growth was continuously changing, reaching a constant growth direction within a distance which was less than sheet thickness but much larger than the estimated craze zone size (approximately 6800 $\overset{o}{A}$). The crack surfaces showed that the crack velocity increased as the crack initially propagated and then crack velocity decreased as the crack approached the long edge of the sheet.

While it is believed the study presented here provides a basis for tracing certain aspects of microcrack growth in fibrous composites, extensive work is still required to completely understand the problem. A wider range of fiber flexibility and geometry should be examined. The nature of arrest for cracks propagating normal to the fibers should also be studied. The flexible fiber model could also be extended by a more realistic three-dimensional model.

To predict crack growth direction in the three-dimensional case, the interaction of all three crack displacement modes will have to be explored. The finite element method may prove to be promising in this problem, in conjunction with the total energy release rate criterion. This criterion itself needs further experimental verification, especially with materials other than rigid plastics.

91

ACKNOWLEDGMENTS

REFERENCES

1) G. Lubin, Handbook of Fiberglass and Advanced Plastics Composites, Van Nostrand Reinhold Co., (1969).

2) L. Holliday, Composite Materials, Elsevier Publishing Co., (1969).

3) S.W. Beckwith, R.A. Schapery and L.D. Webb, Literature Survey of the Field of Fiber-Reinforced Plastic Composites, Parts I&II, Texas A&M University, CMR I&II, (1971).

4) S.W. Tsai, J.C. Halpin and N.J. Pagano, Composite Materials Workshop, Technomic Publishing Co., Inc., (1968).

5) J.E. Ashton, J.C. Halpin and P.H. Petit, Primer on Composite Materials: Analysis, Technomic Publishing Co., Inc., (1969).

6) Y.C. Lou and R.A. Schapery, "Viscoelastic Characterization of a Nonlinear Fiber-Reinforced Plastic," Journal of Composite Materials, 5 (1971) 208.

7) J.E. Ashton, "Non-Linear Viscoelastic Response of Fibrous Composites", Journal of Composite Materials, 2 (1968) 116.

8) R.A. Schapery, S.W. Beckwith and N. Conrad, "Studies on the Viscoelastic Behavior of Fiber-Reinforced Plastic," Air Force Materials Laboratory, AFML-TR-73-179, (1973).

9) R.A. Schapery, "Viscoelastic Behavior and Analysis of Composite Materials," Texas A&M University, MM-72-3, (1972).

10) S.W. Beckwith, "Viscoelastic Characterization of a Nonlinear, Glass/ Epoxy Composite Including the Effects of Damage," Texas A&M University, MM-2895-74-8, (1974).

11) T. Tanimoto and S. Amijima, "Progressive Nature of Fatigue Damage of Glass Fiber Reinforced Plastics," Journal of Composite Materials, 9 (1975) 380.

12) B.W. Rosen and N.F. Dow, "Mechanics of Failure of Fibrous Composites," Fracture, Vol. VII, H. Liebowitz Ed., Academic Press, (1968).

13) H.T. Corten, "Fracture Mechanics of Composites," Fracture, Vol. VII, H. Liebowitz, Ed., Academic Press, (1968).

14) J.T. Paul and J.B. Thomson, "The Importance of Voids in the Filament-Wound Structure," Proceedings of the 20th Annual Meeting of the Reinforced Plastics Division of the Scoeity of the Plastics Industry, Inc., (1965).

15) S.W. Beckwith, "A Review of Fiber-Reinforced Composite Material Failure Criteria", Texas A&M University, MM-72-7, (1972).

16) J.M. Berry and J.V. Mullin, "The Role of Bond Strenth in the Fracture of Advanced Filament Reinforced Composites " Composite Materials: Testing and Design, ASTM, STP 460, (1969).

17) A.S. Tetelman, "Fracture Processes in Fiber Composite Materials," Composite Materials: Testing and Design, ASTM, STP 460, (1969).

18) F. Erdogan, "Fracture Problems in Composite Materials," Engineering Fracture Mechanics 4 (1974) 811.

19) D.B. Bogg, "On the Plane Elastostatic Problem of a Loaded Crack Terminating at a Material Interface," Journal of Applied Mechanics, 38 (1971) 911.

20) D.O. Swenson and C.A. Rau, "The Stress Distribution Around a Crack Perpendicular to an Interface Between Materials," International Journal of Fracture Mechanics, 6 (1970) 357.

21) P.D. Hilton and G.C. Sih, "A Laminate Composite With a Crack Normal to the Interfaces," International Journal of Solids and Structures, 7 (1970) 913.

22) E.M. Wu, "Application of Fracture Mechanics to Anisotropic Plates," Journal of Applied Mech., 34 (1967) 967.

23) E.M. Wu, "Some Unique Crack Propagation Phenomena to Unidirectional Composites and Their Mathematical Characterization," Structure, Solid Mechanics and Engineering Design, M. Teleni, Ed., Wiley-Interscience, (1969).

24) R.A. Schapery, "A Theory of Crack Growth in Viscoelastic Media," Texas A&M University, MM 2764-73-1, (1973).

25) F.A. McClintock, "Plasticity Aspects of Fracture," Fracture, Vol. VI, H. Liebowitz, Ed., Academic Press, (1968).

26) A.A. Griffith, "The Phenomena of Rupture and Flow in Solids," Transactions, Royal Soc. London, 221 (1920) 163.

27) C.E. Inglis, "Stresses in a Plate Due to the Preserve of Cracks and Sharp Corners," Proceedings, Inst. Naval Architects, 60 (1913) 10.

28) I.N. Sneddon, "The Distribution of Stress in the Neighborhood of a Crack in an Elastic Solid," Proceedings, Royal Soc. London, A-187 (1946) 52.

29) G.R. Irwin, "Analysis of Stresses and Strains Near the End of a Crack Traversing a Plate," Journal of Applied Mechanics, 23 (1957) 143.

30) G.R. Irwin, "Fracture," Handbuch der Physik, Vol. VI, Springer, (1958).

31) M.L. Williams, "On the Stress Distribution at the Base of a Stationary Crack," Journal of Applied Mechanics, 24 (1957) 118.

32) H.M. Westergaard, "Bearing Pressures and Cracks," Journal of Applied Mechanics, 6 (1939) 206.

33) G.R. Irwin, "Fracture Mechanics," Structural Mechanics, Pergamon Press, (1960).

34) R.A. Schapery, "A Theory of Crack Initiation and Growth in Visco-elastic Media III. Analysis of Continuous Growth," International Journal of Fracture, 11 (1975) 556.

35) P.C. Paris, "Stress-Intensity Factors by Dimensional Analysis," Lehigh University, (1961).

36) P.C. Paris and G.C. Sih, "Stress Analysis of Cracks," Fracture Toughness Testing and its Applications, ASTM, STP 381, (1965).

37) H. Tada, The Stress Analysis of Cracks Handbook, Del Research Corp., (1973).

38) G.C. Sih, Handbook of Stress - Intensity Factors, Lehigh University, (1973).

39) A.S. Kobayashi and R.D. Cherepy, "A Numerical Procedure for Estimating the Stress Intensity Factor of a Crack in a Finite Plate," Journal of Basic Engineering, Trans., ASME, 86 (1964) 681.

40) W.K. Wilson, "Numerical Method for Determining Stress Intensity Factors of an Interior Crack in a Finite Plate," Journal of Basic Engineering, Trans., ASME, 93 (1973) 685.

41) O.C. Zienkiewicz, The Finite Element Method in Engineering Science, McGraw-Hill, (1971).

42) S.K. Chan, I.S. Tuba and W.K. Wilson, "On the Finite Element Method in Linear Fracture Mechanics," Engineering Fracture Mechanics, 2 (1970) 1.

43) J.J. Oglesby and O. Lomacky, An Evaluation of Finite Element Methods for the Computation of Elastic Stress Intensity Factors, NSRDC Report 3751, (1971).

44) P.D. Hilton and G.C. Sih, "Applications of the Finite Element Method to the Calculations of Stress Intensity Factors," Methods of Analysis and Solutions of Crack Problems, G.C. Sih, Ed., Noordhoff, (1973).

45) C.L. Chow and K.J. Lau, "On the Finite Element Method for Calculating Stress Intensity Factors with a Modified Elliptical Model," International Journal of Fracture, 12, (1976) 59.

46) W.K. Wilson, "Finite Element Methods for Elastic Bodies Containing Cracks," Methods of Analysis and Solutions of Crack Problems, G.C. Sih, Ed., Noordhoff, (1973).

47) J.R. Rice, "Mathematical Analysis in the Mechanics of Fracture," Fracture, Vol. II, H. Liebowitz, Ed., Academic Press, (1971).

48) A.S. Kobayashi, S.T. Chiu and R. Beeuwkes, "A Numerical and Experimental Investigation on the Use of the J-Integral," Engineering Fracture Mechanics, 5 (1973) 293.

49) B.K. Neale, "Finite Element Crack Tip Modelling When Evaluating the J-Integral," International Journal of Fracture, 11 (1975) 177.

50) M. Stern and M.L. Soni, "The Calculation of Stress Intensity Factors in Anisotripic Materials by a Contour Integral Method," Computational Fracture Mechanics, ASME, (1975).

51) V.B. Watwood, "The Finite Element Method for Prediction of Crack Behavior," Nuclear Engineering and Design, 11 (1969) 323.

52) G.P. Anderson, V.L. Ruggles and G.S. Stibor, "Use of Finite Element Computer Programs in Fracture Mechanics," International Journal of Fracture Mechanics, 7 (1973) 421.

53) G.P. Anderson and M.L. Williams, "Finite Elements in Adhesion Analyses," International Journal of Fracture, 9 (1973) 421.

54) J.K. Helen and W.S. Blackburn, "The Calculation of Stress Intensity Factors in Two and Three-Dimensions Using Finite Elements," Computational Fracture Mechanics, ASME, (1975).

55) L.P. Pook and J.R. Dixon, "Stress Intensity Factors Calculated Generally by the Finite Element Technique," Nature, 224 (1969) 166.

56) W.K. Wilson, Combined Mode Fracture Mechanics, Ph.D. Dissertation, University of Pittsburgh, (1969).

57) P.D. Hilton and J.W. Hutchinson, "Plastic Intensity Factors for Cracked Plates," Engineering Fracture Mechanics, 3 (1971) 435.

58) W.K. Wilson, "Some Crack Tip Finite Elements for Plane Elasticity," Stress Analysis and Growth of Cracks, ASTM, STP 513, (1972).

59) E. Byskov, "The Calculation of Stress Intensity Factors Using the Finite Element Method with Cracked Element," International Journal of Fracture Mechanics, 6 (1970) 159.

60) P.F. Walsh, "The Computation of Stress Intensify Factors By a Special Finite Element Technique," *International Journal of Solids and Structures*, 7 (1971) 133.

61) Y. Yamamoto, Y. Sumi and K. Ao, "Stress Intensity Factors From Semi-Elliptical Side Notches in Plates," *International Journal of Fracture*, 10 (1974) 593.

62) P. Tong, T.H.H. Pian and S.J. Lasry, "A Hybrid-Element Approach to Crack Problems in Plane Elasticity," *International Journal for Numerical Methods in Engineering*, 7 (1973) 297.

63) P. Tong and T.H.H. Pian, "On the Convergence of the Finite Element Method for Problems with Singularity," *International Journal of Solids and Structures*, 9 (1973) 313.

64) K.Y. Lon, P. Tong and O. Orringer, "Effect of Shape and Size on Hybrid Crack-Containing Finite Elements," *Computational Fracture Mechanics*, ASME, (1975).

65) S.N. Atluri, A.S. Kobayashi and M. Nakagaki, "An Assumed Displacement Hybrid Finite Element Model for Linear Fracture Mechanics," *International Journal of Fracture*, 11, (1975) 257.

66) J.R. Koteras, *A Hybrid Finite Element For Determination of Stress Intensity Factors at a Crack Tip*, University of Texas, TICOM-73-2, (1973).

67) D.M. Tracey, "Finite Elements for Determination of Crack Tip Elastic Stress Intensity Factors," *Engineering Fracture Mechanics*, 3 (1971) 255.

68) H.D.H. Henshell and K.G. Shaw, "Crack Tip Finite Elements are Unnecessary," *International Journal for Numerical Methods in Engineering*, 9 (1975) 495.

69) R.S. Barsoum, "Application of Quadratic Isoparametric Finite Elements in Linear Fracture Mechanics," *International Journal of Fracture*, 10 (1974) 603.

70) J.M. Bloom, "An Evaluation of a New Crack Tip Element - The Distorted 8-Node Isoparametric Element," *International Journal of Fracture*, 11 (1975) 705.

71) J.M. Bloom and D.B. Van Fossen, "An Evaluation of the 20-Node Quadratic Isoparametric Singularity Brick Element," *International Journal of Fracture*, 12 (1976) 161.

72) D.J. Hayes, "A Practical Application of Buckner's Formulation for Determining Stress Intensity Factors for Cracked Bodies," *International Journal of Fracture Mechanics*, 8 (1972) 157.

73) P.C. Paris and R.M. McMeeking, "Efficient Finite Element Methods for Stress Intensity Factors Using Weight Functions," _International Journal of Fracture_, 11 (1975) 354.

74) A.F. Emery, F.J. Cupps and P.K. Neighbors, "The Use of Singularity Programming in Finite-Element Calculations of Elastic Intensity Factors, Plane and Axisymmetric - Applied to Thermal Stress Fracture," _Computational Fracture Mechanics_, ASME, (1975).

75) P.F. Walsh, "Cracks, Notches, and Finite Elements," _Computational Fracture Mechanics_, ASME, (1975).

76) K. Ando, "Analysis For Cracks in Ship Structures Using the Finite Element Method with the Concept of Crack Sub-Structure," _Computational Fracture Mechanics_, ASME, (1975).

77) P. Nair and K.L. Reifsnider, "Unimod: An Applications Oriented Finite Element Scheme for the Analysis of Fracture Mechanics Problems," _Fracture Analysis_, ASTM, STP 560, (1974).

78) N. Levy, P.V. Marcal and J.R. Rice, "Progress in Three Dimensional Elastic-Plastic Stress Analysis for Fracture Mechanics," _Nuclear Engineering and Design_, 17 (1971) 61.

79) P.F. Walsh, "Linear Fracture Mechanics in Orthotropic Materials," _Engineering Fracture Mechanics_, 4 (1972) 533.

80) S.G. Papaioanrou, P.D. Hilton and R.A. Lucas, "A Finite Element Method for Calculating Stress Intensity Factors and Its Application to Composites," _Engineering Fracture Mechanics_, 6 (1974) 807.

81) S.N. Alturi, A.S. Kobayashi and M. Nakagaki, "A Finite-Element Program for Fracture Mechanics Analysis of Composite Material," _Fracture Mechanics of Composites_, ASTM, STP 593, (1975).

82) F. Erdogan and G.C. Sih, "On the Crack Extension in Plates Under Plane Loading and Transverse Shear," _Journal of Basic Engineering_, 85 (1963) 519.

83) J.G. Williams and P.D. Ewing, "Fracture Under Complex Stress - The Angled Crack Problem," _International Journal of Fracture Mechanics_, 8 (1972) 446.

84) I. Finnie and A. Saith, "A Note on the Angled Crack Problem and the Directional Stability of Cracks," _International Journal of Fracture_, 9 (1973) 484.

85) P.D. Ewing and J.G. Williams, "Further Observations on the Angled Crack Problem," _International Journal of Fracture_, 10 (1974) 135.

86) P.D. Ewing, J.L. Swedlow and J.G. Williams, "Further Results on the Angled Crack Problem," _International Journal of Fracture_, 12(1976)85.

87) G.C. Sih and M.E. Kipp, "Discussion," International Journal of Fracture, 10 (1974) 261.

88) G.C. Sih, Some Basic Problems in Fracture Mechanics and New Concepts, Lehigh University, IFSM-70-16, (1972).

89) G.C. Sih, Application of Strain-Energy-Density Theory to Fundamental Fracture Problems, Lehigh University, IFSM-73-49, (1973).

90) G.C. Sih, Strain-Energy-Density Factor Applied to Mixed Mode Crack Problems, Lehigh University, IFSM-74-54, (1974).

91) I. Finnie and H.D. Weiss, "Some Observations on Sih's Strain Energy Density Approach for Fracture Prediction," International Journal of Fracture, 10 (1974) 136.

92) P. Palaniswamy and W.G. Knauss, On the Problem of Crack Extension in Brittle Solids Under General Loading, California Institute of Technology, SM-74-8, (1974).

93) G.C. Sih, "Discussion," International Journal of Fracture, 10 (1974) 279.

94) P.H. Francis and W.L. Ko, "The Effect of Root Radius on the Direction of Crack Extension Under Combined Mode Loading," Internation Journal of Fracture, 10 (1976) 243.

95) M.A. Hussain, S.L. Pu and J. Underwood, "Strain Energy Release Rate for a Crack Under Combined Mode I and Mode II," Fracture Analysis, ASTM, STP 560, (1974).

96) J. Coughlan and B.I.G. Barr, "Future Crack Prediction," International Journal of Fracture, 10 (1974) 590.

97) S.A. Marishaw and G.H. Lindsey, "Plane Stress Crack Trajectories in Low Modulus Materials," International Journal of Fracture, 11 (1975) 273.

98) T.K. Helen and W.S. Blackburn, "The Calculation of Stress Intensity Factors for Combined Tensile and Shear Loading," International Journal of Fracture, 11 (1975) 605.

99) B.A. Bilby and G.E. Cardew, "The Crack With a Kinked Tip," International Journal of Fracture, 11 (1975) 708.

100) A.A. Khrapkov, "The First Basic Problem for a Notch at the Apex of an Infinite Wedge," International Journal of Fracture Mechanics, 7 (1971) 373.

101) E.M. Morozov and Y.A.B. Fridman, "Trajectories of Brittle-Fracture Cracks as Geodesic Lines on the Surface of a Body," Soviets Physics Doklody, 6 (1962) 619.

102) G.H. Lindsey, "Some Observations on Fracture Under Combined Load-
ing," Progress in Flaw Growth and Fracture Toughness Testing,
ASTM, STP 536, (1973).

103) R.J. Nuismer, "An Energy Release Rate Criterion for Mixed Mode
Fracture," International Journal of Fracture, 11 (1975) 245.

104) H. Lee and K. Neville, Encyclopedia of Polymer Science and
Technology, Vol. 6, John Wiley and Sons, Inc., (1964).

105) R.J. Meyers and L.S. Luskins, Encyclopedia of Polymer Science and
Technology, Vol. 1, John Wiley and Sons, Inc., (1964).

106) E.H. Andrews, Fracture in Polymers, Oliver and Boyd, Ltd. (1968).

107) J.P. Berry, "Fracture of Polymeric Glasses," Fracture, Vol. VII,
H. Liebowitz, Ed., Academic Press, (1968).

108) S. Mostovoy and E.J. Ripling, "Fracture Toughness of an Epoxy
System," Journal of Applied Polymer Science, 10 (1966) 1351.

109) G. Epstein and W. Bandarak, "The Crazing Phenomenon and Its Effects
in Filament-Would Pressure Vessels," Proceedings of the 19th
Annual Meeting of the Reinforced Plastics Division of the Society
of the Plastics Industry, Inc., (1964).

110) R.P. Kambour, "Mechanism of Fracture in Glassy Polymers. I. Frac-
ture Surfaces in Polymethyl Methacrylate," Journal of Polymer
Science: Part A, 3 (1965) 1713.

111) R.P. Kambour, "Mechanism of Fracture in Glassy Polymers. II. Sur-
vey of Crazing Response During Crack Propagation in Several Poly-
mers," Journal of Polymer Science: Part A-2, 4 (1966) 17.

112) R.P. Kambour, "Mechanism of Fracture in Glassy Polymers.
III. Direct Observation of the Craze Ahead of the Propagating
Crack in Poly (Methyl Methacrylate) and Polystyrene," Journal
of Polymer Science: Part A-2, 4 (1966) 349.

113) R.P. Kambour and R.E. Barker, Jr., "Mechanism of Fracture in
Glassy Polymers. IV. Temperature Rise at the Tip of Propagating
Crack in Poly (Methyl Methacrylate)," Journal of Polymer Science:
Part A-2, 4 (1966) 359.

114) G.P. Marshall, L.E. Culver, and J.G. Williams, "Crack and Craze
Propagation in Polymers: A Fracture Mechanics Approach,"
Plastics and Polymers, 37 (1969) 75.

115) J.G. Williams, "Visco-Elastic and Thermal Effects on Crack Growth
in PMMA," International Journal of Fracture Mechanics, 8 (1972)
393.

116) J.J. Benbow, "Stable Crack Propagation in Plastics," Proceedings of the Physics Society, 78 (1961) 970.

117) "Plexiglas Sheet Physical Properties," PL-229L report, obtained from J.M. Rowan, Rohm and Haas Company, Houston, April 1975.

118) Information furnished by Micro-Measurements, Romulas, Michigan, Sept. 1975.

119) C.N. Freed, A.M. Sullivan and J. Stoop, "Influence of Dimensions of the Center-Cracked Tension Specimen on K_c," Fracture Toughness, Proceedings of the 1971 National Symposium on Fracture Mechanics, Part II, ASTM, STP 514, (1972).

120) T.W. Orange, "Some Effects of Experimental Error in Fracture Testing," Fracture Analysis, ASTM, STP 560, (1974).

121) H.K. Mueller, "Stress-Intensity Factor and Crack Opening for a Linearly Viscoelastic Strip with a Slowly Propagating Central Crack," International Journal of Fracture Mechanics, 7 (1971) 129.

122) M.L. Williams, P.J. Blatz and R.A. Schapery, Fundamental Studies Relating to Systems Analysis of Solid Propellants, California Institute of Technology, GALCIT SM 61-5, (1961).

123) J.D. Ferry, Viscoelastic Properties of Polymers, John Wiley and Sons, Inc., (1970).

124) G.R. Booker, "Scanning Electron Microscopy - The Instrument," Modern Diffraction and Imaging Techniques in Material Science, S. Amelinckx, Ed., North Holland Publishing Co., (1970).

125) H.J. Kornish, J.L. Swedlow and T.A. Cruse, "Experimental Investigation of Fracture in an Advanced Fiber Composite," Journal of Composite Materials, 6 (1972) 114.

126) C.A. Berg and A. Rinsky, "Tensile Fracture of Graphite Fiber Reinforced Epoxy Composites," Fibre Science and Technology, 3 (1971) 295.

127) A.R. Rosenfield and P.N. Mincer, "Crack Propagation and Arrest in Polymethymethacrylate," Polymer Science Symposium No. 32, John Wiley and Sons, Inc., (1971).

128) J.P. Berry, "Fracture Processes in Polymeric Materials. III. Topography of Fracture Surfaces of Poly (Methyl Methacrylate)," Journal of Applied Physics, 33 (1962) 1741.

129) C.S. Desai and J.F. Abel, Introduction to the Finite Element Method, Van Nostrand Reinhold Co., (1972).

130) T.H. Pian and O. Orringer, Massachusetts Institute of Technology, private communication, 1974.

131) R.S. Dunham and E.B. Becker, TEXGAP - The Texas Grain Analysis Program, University of Texas, TICOM 73-1, (1973).

132) M. Hetenyi, Beams on Elastic Foundation, University of Michigan Press, (1946).

133) G.C. Sih, P.C. Paris and G.R. Irwin, "On Cracks in Rectilinearly Anisotropic Bodies," International Journal of Fracture Mechanics, 1 (1965) 189.

APPENDIX

Effective Properties

The effective properties of the orthotropic material can be derived from the properties of the constituent materials by various means. There are various theories proposed that are based on descrete element models, variational principles, semi-empirical approaches and others. These methods can be found in [3]. The method used here is the descrete element model. Here, each constituent, fiber and matrix, is considered separately and the sum of their individual contributions is assumed to be the same as that of the orthotropic material. The overall stress-strain relationship used here is for an orthotropic body in plane stress as in [142].

$$\varepsilon_i = \sum_{j=1}^{6} a_{ij} \sigma_j, \ a_{ij} = a_{ji} \ , \ (i,j=1,2,6)$$

$$\varepsilon_1 = \varepsilon_x, \ \varepsilon_2 = \varepsilon_y, \ \varepsilon_6 = \gamma_{xy} \qquad\qquad (A-1)$$

$$\sigma_1 = \sigma_x, \ \sigma_2 = \sigma_y, \ \sigma_6 = \tau_{xy}$$

First, an element of the material is considered to be in uniform strain parallel to the fibers. One considers the forces in each fiber and matrix section, and sets the sum of all the forces in the individual fiber and matrix sections equal to the overall force. This gives the stiffness in the fiber direction in terms of the volume fractions of the constituents.

$$\frac{1}{a_{11}} = E_f \, V_f + E_m \, V_m \qquad\qquad (A-2)$$

By considering the lateral contraction of the overall material, one can determine that

$$\nu_{12} = \nu_m V_m + \nu_f V_f \tag{A-3}$$

with (A-1) and (A-2) one finds

$$a_{12} = \nu_{12} \, a_{11} \tag{A-4}$$

By considering an element of the material in simple shear parallel to the fibers, the shear stresses in each constituent is the same. The values of the shear displacement in each fiber and matrix section is summed and set equal to the overall shear displacement. In terms of the fiber and matrix shear modulus one finds

$$a_{66} = \frac{V_f}{G_f} + \frac{V_m}{G_m} \tag{A-5}$$

For the compliance of the material perpendicular to the fibers, one can consider an element of the material to be loaded by an overall force perpendicular to the fibers and with no overall force parallel to the fibers. By adding the displacements perpendicular to the fibers, for each fiber and matrix section, and setting the sum equal to the overall displacement of the element, one can derive

$$a_{22} = \frac{V_m}{E_m} \left[1 - \frac{\nu_m (\nu_m E_f - \nu_f E_m)}{E_f + \frac{E_m V_m}{V_f}} \right] +$$

$$\tag{A-6}$$

$$\frac{V_f}{E_f} \left[1 - \frac{\nu_f (\nu_f E_m - \nu_m E_f)}{E_m + E_f \frac{V_f}{V_m}} \right]$$

These compliances were used as the effective properties of the continuum composite model in equation (27).

Naval Ship Research & Development Center
Annapolis Division
Annapolis, MD 21402

Attn: Code 28 - Mr. R.J. Wolfe

Naval Ship Research & Development Center
Annapolis Division
Annapolis, MD 21402

Attn: Code 281 - Mr. R.B. Nierderberger

Naval Ship Research & Development Center
Annapolis Division
Annapolis, MD 21402

Attn: 2814 - Dr. H. Vanderveldt

Technical Library
Naval Underwater Weapons Center
Pasadena Annex
3202 E. Foothill Blvd.
Pasadena, CA 91107

U.S. Naval Weapons Center
China Lake, CA 93557

Attn: Code 4062 - Mr. W. Werback

U.S. Naval Weapons Center
China Lake, CA 93557

Attn: Code 4520 - Mr. Ken Bischel

Commanding Officer
U.S. Naval Civil Engr. Lab.
Code L31
Port Hueneme, CA 93041

Technical Director
U.S. Naval Ordnance Laboratory
White Oak
Silver Spring, MD 20910

Technical Director
Naval Undersea R&D Center
San Diego, CA 92132

Supervisor of Shipbuilding
U.S. Navy
Newport News, VA 23607

Technical Director
Mare Island Naval Shipyard
Vallejo, CA 94592

U.S. Navy Underwater Sound Ref. Lab.
Office of Naval Research
P.O. Box 8337
Orlando, FL 32806

Chief of Naval Operations
Dept. of the Navy
Washington, D.C. 20350

Attn: Code Op07T

Strategic Systems Project Office
Department of the Navy
Washington, D.C. 20390

Attn: NSP-001 Chief Scientist

Deep Submergence Systems
Naval Ship Systems Command
Code 39522
Department of the Navy
Washington, D.C. 20360

Engineering Dept.
U.S. Naval Academy
Annapolis, MD 21402

Naval Air Systems Command
Dept. of the Navy
Washington, D.C. 20360

Attn: NAVAIR 5302 Aero & Structures

Naval Air Systems Command
Dept. of the Navy
Washington, D.C. 20360

Attn: NAVAIR 5308 Structures

Naval Air Systems Command
Dept. of the Navy
Washington, D.C. 20360

Attn: NAVAIR 52031F Materials

Naval Air Systems Command
Dept. of the Navy
Washington, D.C. 20360

Attn: NAVAIR 604 Tech. Library

DISTRIBUTION LIST

Chief of Naval Research
Department of the Navy
Arlington, VA 22217

Attn: Code 474   (2)

Chief of Naval Research
Department of the Navy
Arlington, VA 22217

Attn: Code 471

Chief of Naval Research
Department of the Navy
Arlington, VA 22217

Attn: Code 222

Director
ONR Branch Office
495 Summer Street
Boston, MA 02210

Director
ONR Branch Office
219 S. Dearborn Street
Chicago, IL 60604

Director
Naval Research Laboratory
Attn: Code 2629 (ONRL)
Washington, D.C. 20390   (6)

U. S. Naval Research Laboratory
Attn: Code 2627
Washington, D. C. 20390

Director
ONR - New York Area Office
715 Broadway - 5th Floor
New York, NY 10003

Director
ONR Branch Office
1030 E. Green Street
Pasadena, CA 91101

Defense Documentation Center
Cameron Station
Alexandria, VA 22314   (12)

Commanding Officer
U.S. Army Research Office Durham
Attn: Mr. J. J. Murray
CRD-AA-IP
Box CM, Duke Station
Durham, NC 27706   (2)

Commanding Officer
AMXMR-ATL
Attn: Mr. R. Shea
U.S. Army Materials Res. Agency
Watertown, MA 02172

Watervliet Arsenal
MAGGS Research Center
Watervliet, NY 12189

Attn: Director of Research
         Technical Library

Redstone Scientific Info. Center
Chief, Document Section
U.S. Army Missile Command
Redstone Arsenal, AL 35809

Army R&D Center
Fort Belvoir, VA 22060

Commanding Officer and Director
Naval Ship Research & Development Center
Bethesda, MD 20034

Attn: Code 042 (Tech. Lib. Br.)

Commanding Officer and Director
Naval Ship Research & Development Center
Bethesda, MD 20034

Attn: Code 17 (Struc. Mech. Lab.)

Commanding Officer and Director
Naval Ship Research & Development Center
Bethesda, MD 20034

Attn: Code 172

Commanding Officer and Director
Naval Ship Research & Development Center
Bethesda, MD 20034

Attn: Code 172

Naval Ship Engineering Center
Prince George's Plaza
Hyattsville, MD 20782

Attn: NAVSEC 6129 Submarine Struct.

Commander WADD
Wright-Patterson Air Force Base
Dayton, OH 45433

Attn: Code WWRMDD

Commander WADD
Wright-Patterson Air Force Base
Dayton, OH 45433

Attn: Code AFFDL (FDDS)

Commander WADD
Wright-Patterson Air Force Base
Dayton, OH 45433

Attn: Structures Division

Commander WADD
Wright-Patterson Air Force Base
Dayton, OH 45433

Attn: AFLC (MCEEA)

Chief, Applied Mechanics Group
U.S. Air Force Inst. of Tech.
Wright-Patterson Air Force Base
Dayton, Ohio 45433

Chief, Civil Engineering Branch
WLRC, Research Division
Air Force Weapons Laboratory
Kirtland AFB, New Mexico 87117

Air Force Office of Scientific Research
1400 Wilson Blvd.
Arlington, VA 22209

Attn: Mechanics Div.

Structures Research Division
National Aeronautics & Space Admin.
Langley Research Center
Langley Station
Hampton, VA 23365

National Aeronautic & Space Admin.
Associate Administrator for Advanced
  Research & Technology
Washington, D.C. 02546

Scientific & Tech. Info. Facility
NASA Representative (S-AK/DL)
P.O. Box 5700
Bethesda, MD 20014

Commandant
Chief, Testing & Development Div.
U.S. Coast Guard
1300 E. Street, N.W.
Washington, D.C. 20226

Technical Director
Marine Corps Dev. & Educ. Command
Quantico, VA 22134

Director
National Bureau of Standards
Washington, D.C. 20234

Attn: Mr. B.L. Wilson, EM 219

Dr. M. Gaus
National Science Foundation
Engineering Division
Washington, D.C. 20550

Science & Tech. Division
Library of Congress
Washington, D.C. 20540

Director
Defense Nuclear Agency
Washington, D.C. 20305

Attn: SPSS

Commander Field Command
Defense Nuclear Agency
Sandia Base
Albuquerque, NM 87115

Director Defense Research & Engrg
Technical Library
Room 3C-128
The Pentagon
Washington, D.C.

Commanding Officer and Director
Naval Ship Research & Development Center
Bethesda, MD 20034

Attn: Code 174

Commanding Officer and Director
Naval Ship Research & Development Center
Bethesda, MD 20034

Attn: Code 177

Commanding Officer and Director
Naval Ship Research & Development Center
Bethesda, MD 20034

Attn: Code 1800 (Appl. Math. Lab.)

Commanding Officer and Director
Naval Ship Research & Development Center
Bethesda, MD 20034

Attn: Code 5412S (Dr. W.D. Sette)

Commanding Officer and Director
Naval Ship Research & Development Center
Bethesda, MD 20034

Attn: Code 19 (Dr. M.M. Sevik)

Commanding Officer and Director
Naval Ship Research & Development Center
Bethesda, MD 20034

Attn: Code 1901 (Dr. M. Strassberg)

Commanding Officer and Director
Naval Ship Research & Development Center
Bethesda, MD 20034

Attn: Code 1945

Commanding Officer and Director
Naval Ship Research & Development Center
Bethesda, MD 20034

Attn: Code 196 (Dr. D. Feit)

Commanding Officer and Director
Naval Ship Research & Development Center
Bethesda, MD 20034

Attn: Code 1962

Naval Weapons Laboratory
Dahlgren, VA 22448

Naval Research Laboratory
Washington, D.C. 20375

Attn: Code 8400

Naval Research Laboratory
Washington, D.C. 20375

Attn: Code 8410

Naval Research Laboratory
Washington, D.C. 20375

Attn: Code 8430

Naval Research Laboratory
Washington, D.C. 20375

Attn: Code 8440

Naval Research Laboratory
Washington, D.C. 20375

Attn: Code 6300

Naval Research Laboratory
Washington, D.C. 20375

Attn: Code 6390

Naval Research Laboratory
Washington, D.C. 20375

Attn: Code 6380

Undersea Explosion Research Div.
Naval Ship R&D Center
Norfolk Naval Shipyard
Portsmouth, VA 23709

Attn: Dr. E. Palmer
        Code 780

Naval Ship Research & Development Center
Annapolis Division
Annapolis, MD 21402

Attn: Code 2740 - Dr. Y.F. Wang

Naval Air Systems Command
Dept. of the Navy
Washington, D.C. 20360

Attn: NAVAIR 320B Structures

Director, Aero Mechanics
Naval Air Development Center
Johnsville
Warminster, PA 18974

Technical Director
U.S. Naval Undersea R&D Center
San Diego, CA 92132

Engineering Department
U.S. Naval Academy
Annapolis, MD 21402

Naval Facilities Engineering Command
Dept. of the Navy
Washington, D.C. 20360

Attn: NAVFAC 03 Research & Development

Naval Facilities Engineering Command
Dept. of the Navy
Washington, D.C. 20360

Attn: NAVFAC 04 Research & Development

Naval Facilities Engineering Command
Dept. of the Navy
Washington, D.C. 20360

Attn: NAVFAC 14114 Tech. Library

Naval Sea Systems Command
Dept. of the Navy
Washington, D.C. 20360

Attn: NAVSHIP 03 Res. & Technology

Naval Sea Systems Command
Dept. of the Navy
Washington, D.C. 20360

Attn: NAVSHIP 031 Ch. Scientist for R&D

Naval Sea Systems Command
Dept. of the Navy
Washington, D.C. 20360

Attn: NAVSHIP 03412 Hydromechanics

Naval Sea Systems Command
Dept. of the Navy
Washington, D.C. 20360

Attn: NAVSHIP 037 Ship Silencing Div.

Naval Sea Systems Command
Dept. of the Navy
Washington, D.C. 20360

Attn: NAVSHIP 035 Weapons Dynamics

Naval Ship Engineering Center
Prince George's Plaza
Hyattsville, MD 20782

Attn: NAVSEC 6100 Ship Sys Engr & Des Dep

Naval Ship Engineering Center
Prince George's Plaza
Hyattsville, MD 20782

Attn: 6102C Computer-Aided Ship Design

Naval Ship Engineering Center
Prince George's Plaza
Hyattsville, MD 20782

Attn: 6105G

Naval Ship Engineering Center
Prince George's Plaza
Hyattsville, MD 20782

Attn: NAVSEC 6110 Ship Concept Design

Naval Ship Engineering Center
Prince George's Plaza
Hyattsville, MD 20782

Attn: NAVSEC 6120 Hull Div.

Naval Ship Engineering Center
Prince George's Plaza
Hyattsville, MD 20782

Attn: NAVSEC 6120D Hull Div.

Naval Ship Engineering Center
Prince George's Plaza
Hyattsville, MD 20782

Attn: NAVSEC 6128 Surface Ship Struct.

Chief, Airframe & Equipment Branch
FS-120
Office of Flight Standards
Federal Aviation Agency
Washington, D.C. 20553

Chief, Research and Development
Maritime Administration
Washington, D.C. 20235

Deputy Chief, Office of Ship Constr.
Maritime Administration
Washington, D.C. 20235

Attn: Mr. U.L. Russo

Atomic Energy Commission
Div. of Reactor Devel. & Tech.
Germantown, MD 20767

Ship Hull Research Committee
National Research Council
National Academy of Sciences
2101 Constitution Avenue
Washington, D.C. 20418

Attn: Mr. A.R. Lytle

Dr. J. Tinsley Oden
University of Texas at Austin
345 Eng. Science Bldg.
Austin, Texas 78712

Prof. Julius Miklowitz
California Institute of Technology
Div. of Engineering & Applied Sciences
Pasadena, CA 91109

Dr. Harold Liebowitz, Dean
School of Engr. & Applied Science
George Washington University
725-23rd St., N.W.
Washington, D.C. 20006

Prof. Eli Sternberg
California Institute of Technology
Div. of Engr. & Applied Sciences
Pasadena, CA 91109

Prof. Paul M. Naghdi
University of California
Div. of Applied Mechanics
Etcheverry Hall
Berkeley, CA 94720

Professor P. S. Symonds
Brown University
Division of Engineering
Providence, R.I. 02912

Prof. A. J. Durelli
The Catholic University of America
Civil/Mechanical Engineering
Washington, D.C. 20017

Prof. R.B. Testa
Columbia University
Dept. of Civil Engineering
S.W. Mudd Bldg.
New York, N.Y. 10027

Prof. H.H. Bleich
Columbia University
Dept. of Civil Engineering
Amsterdam & 120th St.
New York, N.Y. 10027

Prof. F.L. DiMaggio
Columbia University
Dept. of Civil Engineering
616 Mudd Building
New York, N.Y. 10027

Prof. A.M. Freudenthal
George Washington University
School of Engineering & Applied Science
Washington, D.C. 20006

D.C. Evans
University of Utah
Computer Science Division
Salt Lake City, WA 84112

Prof. Norman Jones
Massachusetts Inst. of Technology
Dept. of Naval Architecture & Marine
  Engineering
Cambridge, MA 02139

Professor Albert I. King
Biomechanics Research Center
Wayne State University
Detroit, MI 48202

Dr. V. R. Hodgson
Wayne State University
School of Medicine
Detroit, MI 48202

REPORT DOCUMENTATION PAGE

READ INSTRUCTIONS
BEFORE COMPLETING FORM

1. REPORT NUMBER	2. GOVT ACCESSION NO.	3. RECIPIENT'S CATALOG NUMBER
Technical Report No. 2		

4. TITLE (and Subtitle)

ON MICROCRACK GROWTH AND ARREST
IN SIMULATED FIBROUS COMPOSITES

5. TYPE OF REPORT & PERIOD COVERED

Technical Report

6. PERFORMING ORG. REPORT NUMBER

MM-3168-76-10

7. AUTHOR(s)

Nicholas/Conrad

8. CONTRACT OR GRANT NUMBER(s)

N00014-75-C-0325

9. PERFORMING ORGANIZATION NAME AND ADDRESS

Mechanics and Materials Research Center
Texas Engineering Experiment Station
Texas A&M University
College Station, Texas 77843

10. PROGRAM ELEMENT, PROJECT, TASK AREA & WORK UNIT NUMBERS

NR 064-520

11. CONTROLLING OFFICE NAME AND ADDRESS

Office of Naval Research
Dept. of the Navy - 800 N. Qunicy Street
Arlington, Virginia 22217

12. REPORT DATE

December 1976

13. NUMBER OF PAGES

104

14. MONITORING AGENCY NAME & ADDRESS(If different from Controlling Office)

Materials Science Division
Structural Mechanics Program
Code 474

15. SECURITY CLASS. (of this report)

Unclassified

15a. DECLASSIFICATION/DOWNGRADING SCHEDULE

16. DISTRIBUTION STATEMENT (of this Report)

Approved for public release; distribution unlimited

17. DISTRIBUTION STATEMENT (of the abstract entered in Block 20, If different from Report)

18. SUPPLEMENTARY NOTES

19. KEY WORDS (Continue on reverse side if necessary and identify by block number)

20. ABSTRACT (Continue on reverse side if necessary and identify by block number)

Opening, shearing and combined mode fracture tests were conducted with long rectangular strips of plexiglas clamped on the long edges and containing centered and off-centered cracks. The critical stress intensity factors, crack initiation angles, and crack paths were evaluated. Fractured surfaces were then examined as to crack behavior. The maximum energy release rate criterion was extended to problems with a large degree of shearing mode → next page

DD FORM 1473 1 JAN 73   EDITION OF 1 NOV 65 IS OBSOLETE

(Continued from Block 20.)

cont

present. This criterion was then used to predict successfully the initial and subsequent crack propagation behavior presented in the experimental work. Crack arrest was examined for this rigid grip configuration. Using in part information obtained from these studies, a flexible fiber model was investigated to determine the effect of fiber bending on crack behavior. Certain aspects of crack growth and arrest in these idealized fiber models were explored.